Ocean Engineering 257 (2022) 111693

Contents lists available at ScienceDirect

Ocean Engineering

journal homepage: www.elsevier.com/locate/oceaneng

Approximate calculation method of hydrodynamic solution of an array with a large number of truncated cylinders

Xiaohui Zeng [a,b,c], Yuanshun Kang [a,b], Guangyuan Wang [d], Zhen Xue [e], FaJun Yu [e,*]

[a] Institute of Mechanics, Chinese Academy of Sciences, Beijing 100190, China
[b] School of Engineering Science, University of Chinese Academy of Sciences, Beijing 100049, China
[c] State Key Laboratory of Coastal and Offshore Engineering, Dalian University of Technology, Dalian 116024, China
[d] Tianjin Research Institute for Water Transport Engineering, M.O.T, Tianjin 300000, China
[e] Qingdao Innovation and Development Base of Harbin Engineering University, Harbin Engineering University, Qingdao 266000, China

ARTICLE INFO

Keywords:
Approximate calculation method
Truncated cylinders
Added damping coefficients
Added mass coefficients

ABSTRACT

Based on linear wave theory, the hydrodynamic problem of the array of truncated cylinders with relative motion is studied, and the calculation formulas of hydrodynamic force/moment, added mass, and added damping coefficients are given. Firstly, the effect of the evanescent mode on the hydrodynamic coefficients are studied by the truncated two-cylinders as an example. And based on this, an approximation formula for the heave added mass of the truncated two-cylinders is given. After that, a fast formula for calculating the added mass coefficient of an oscillating cylinder of the rectangularly arranged array with a large number of cylinders caused by evanescent mode is presented. Finally, the approximate calculation method of the hydrodynamic coefficients for a large number of rectangular arrays with a given amplitude are summarized. The method is able to efficiently solve the hydrodynamic coefficients of the array with a large number of cylinders, providing an idea to evaluate the performance of such models in engineering.

1. Introduction

In recent years, researchers have proposed various types of floating structures, such as deep-sea platforms, wave energy converts, and offshore wind turbine foundations, due to the need for marine development. Such structures can usually be modeled as isolated truncated cylinders or as arrays of truncated cylinders. Therefore, the diffraction/radiation problem of truncated cylindrical structures has received a lot of research attention.

The first study of the truncated cylinder diffraction problem was conducted by Miles and Gilbert (1968), which was subsequently modified by Garrett (1971). They all applied the idea of region boundary matching. Sabuncu and Calisal (1981) and Yeung (1981) both studied the radiation problem of a truncated cylinder at finite water depth and gave analytical formulas for the added mass and the added damping coefficients of the cylinder for different modes of motion. Bhatta and Rahman (2003) extended the radiation problem of the truncated cylinder at finite water depth to the case with incident waves.

Compared with the isolated truncated cylinder case, the analysis of the radiation problem for truncated cylindrical arrays requires consideration of the interactions between the cylinders, making the solution more difficult. Truncated cylindrical arrays can be divided into two types, oscillation in unison or independently. To solve the problem of diffraction/radiation of multiple three-dimensional bodies, Kagemoto and Yue (1986) combined the direct matrix method (Simon, 1982) and the multiple scattering method (Ohkusu, 1974) to obtain an exact algebraic method. This theory has been used as the basic theory for hydrodynamic analysis of the array of truncated cylinders, taking into account the propagating and evanescent modes between cylinders. Kim (1993) gave the analytical solution of the wave radiation for six-degree-of-freedom motions of N bottom-mounted vertical circular cylinders, which is an extension of Linton and Evans (1990)'s diffraction theory of this model. Yılmaz and Incecik (1998) studied the radiation of truncated cylindrical arrays using the method of Kagemoto and Yue (1986), and gave some results for heave and surge forces. McNatt et al. (2015) proposed a new method for computing the diffraction transfer matrix that significantly reduces the computation time of the Kagemoto and Yue (1986)'s method. The radiation problems of truncated cylindrical arrays that can oscillate independently have also received some attention. Based on the large spacing assumption, Williams and Abul-Azm (1989) investigated the hydrodynamic coefficients of an array of floating cylinders using a modified plane wave technique, where the fluid motion is induced by a prescribed forced oscillation

* Corresponding author.
E-mail address: yufajun@hrben.edu.cn (F. Yu).

https://doi.org/10.1016/j.oceaneng.2022.111693
Received 25 January 2022; Received in revised form 15 April 2022; Accepted 30 May 2022
Available online 14 June 2022

of one of the components. Mavrakos (1991) proposed a more efficient semi-analytical method to study the radiation of arrays of interacting vertical axisymmetric bodies with the relative motion for a given motion case, in which the effect of evanescent modes is taken into account. For truncated four-cylinders with relative motion, Siddorn and Taylor (2008) examined the hydrodynamic characteristics of the array for a given cylinder amplitude and considered the effect of evanescent modes in their analysis. Child and Venugopal (2010) applied the method of Siddorn and Taylor (2008) to study the hydrodynamic response of an array of floating wave energy devices, and based on the improved computational power, the authors used a genetic algorithm to optimize the disposition of the array. The hydrodynamic loads acting on an array of truncated cylinders with each cylinder oscillating independently with different prescribed amplitudes were calculated by Zeng and Tang (2013). Later, Zeng et al. (2016) considered the effect of evanescent modes in his study. The oscillating water column device is also a typical the wave energy conversion, which is an important application of the truncated cylindrical array model. There have been many studies on an array of oscillating water column (OWC) devices, where each device is independent and contains both inner and outer chambers (Konispoliatis and Mavrakos, 2016; Konispoliatis et al., 2016). Progress on truncated cylindrical arrays in the field of wave energy generation can be found in Göteman et al. (2020). Besides, some scholars have also focused on the radiation of non-cylindrical floating structure arrays (Zheng et al., 2019). Kang et al. (2020) conducted numerical and experimental studies on the dumbbell-shaped bridge cofferdam.(Cong et al., 2020) studied Hydrodynamic interaction among multiple columns in front of a vertical wall. Two different solutions have been developed for the calculation of mean drift wave force. One is based on the direct pressure integration and the other is based on the application of momentum conservation theorem in a limited fluid volume surrounding a certain cylinder in the array. To study the hydrodynamic properties of a point-absorbing wave-energy converter (WEC), Zhang et al. (2021b) studied the radiation problem of a floating cylindrical buoy with a hemispherical bottom. Cong et al. (2021) dealt with a new combined concept consisting of an oscillating water column (OWC) device and an offshore wind turbine for the multi-purpose utilization of offshore renewable energy resources. In addition, they developed a self-adaptive Gauss integration method to treat the nearly singular integration that occurs when the field and source points are very close to each other. Real sea conditions are usually more complex, so irregular waves have been studied by many scholars (Grice et al., 2015a,b; Xie et al., 2017; Lu et al., 2020; Sriram et al., 2021). Tromans et al. (1991) first proposed a physical model of New Wave and used the linear superposition of potential flow theory to simulate extreme waves. Zhang et al. (2021a) studied the interaction of focused waves with a fixed vertical cylinder using numerical methods. Interestingly, in recent years, some scholars have focused on the problem of water waves and porous cylindrical arrays (Wang et al., 2022).

Very Large Floating Structures (VLFS), usually with a large number of cylindrical arrays as support structures, have attracted a great deal of interest from researchers in recent years. The excessive number of columns in the array will cause near trapped-mode (Maniar and Newman, 1997; Chatjigeorgiou, 2018; Chatjigeorgiou et al., 2019) on the one hand, resulting in a steep increase in the amplitude of the hydrodynamic force; on the other hand, the conventional method requires a large amount of computer memory and computation time. To overcome the solution difficulties, Murai et al. (1999) proposed a new numerical method to study a very large floating structure supported by several independent cylinders. In this model, the columns can be considered as connected by a thin elastic plate. They applied the method to the hydrodynamic analysis of a 12,000-cylinders structure, but the study neglected the effect of evanescent modes between the cylinders. Later, Kashiwagi (2000) proposed a new hierarchical interaction theory to study the diffraction/radiation phenomenon of a large number of cylindrical arrays considering the evanescent modes. They first dispersed the array into a number of clusters, and then combined these clusters into larger clusters, and repeated this process until the array was formed. Using this method, they evaluated the hydrodynamic characteristic of an array containing 5120 cylinders. Poter and Evans (2005) studied the surface waves of square columns of infinite arrays using multiple Galerkin methods, Rayleigh–Bloch surface waves are described by a localized wave motion which does not propagate energy away from the array. Thompson et al. (2008) proposed a new approximation method for scattering by long finite arrays. and the hydrodynamic results of a single row of 101 columns were calculated. Within the framework of linearization, Garnaud and Mei (2009) considered a periodic array of small buoys with similarly small separation compared to the typical wave length. The method of homogenization (multiple scales) is used to derive the equations governing the macro-scale behavior of the entire array. These equations are then applied to energy extraction by an infinite strip of buoys, and by a circular array. Singh and Babarit (2014) developed a computational approach to investigate wave interaction effects in sparse arrays of floating bodies based on linear water wave theory. And presented the hydrodynamic result of arrays of 50 wave energy converters. Goteman et al. (2015) presented a novel method to model the hydrodynamic interactions and power output of very large wave energy farms, an interaction distance cut-off is introduced to improve the computational cost with acceptable accuracy. Using this approach, they studied the hydrodynamic problems of 252 WECs. A new method is presented to compute the diffraction transfer matrix from plane incident waves by McNatt et al. (2015), they studied a large farm of 101 wave energy converters in regular waves. A hierarchical wave interaction theory is reviewed by Kashiwagi (2017), and introduced experimental results that were obtained using a structure consisting of 64 truncated vertical circular cylinders arranged in a periodical array of 4 rows and 16 columns, this method saves the calculation time effectively. Linear water wave theory is used to study loads imposed on finite line arrays of rigid, bottom-mounted, surface-piercing, vertical cylinders by surface water waves (Bennetts et al., 2017). And an efficient solution method for line arrays is introduced that captures the Rayleigh–Bloch wave modes supported by unperturbed arrays from the scattering characteristics of an individual cylinder. Using this method, they studied the hydrodynamic problems of 200 cylinders. Zeng et al. (2019) proposed an analytical formula for the fluctuation spacing and peak/valley locations of the non-trapped region of the hydrodynamic curve for a large number of bottom-mounted cylinders. Based on this formula, the hydrodynamic envelope curve of the array can be calculated quickly and accurately, which greatly improves the efficiency of structural hydrodynamic assessment.

All of the above studies considered the diffraction/radiation problem for a large number of cylindrical arrays in the presence of incident waves. And at present, there is no simplified method available for preliminary engineering calculations to solve the radiation problem for a large number of truncated cylindrical arrays with relative motion between cylinders of given motion amplitude. In this paper, the arrangement type of cylindrical arrays is divided into three types, and an approximate calculation method for the added mass coefficient caused by the influence of a certain oscillating cylinder suffering from evanescent modes is proposed. The algebraic sum of this value and the added mass coefficient due to the radiative motion of an isolated cylinder is the total added mass coefficient to which the cylinder is subjected. For arrays with multi-cylinder and multi-mode oscillations, the oscillations of each cylinder can be decomposed first and then linearly superimposed. The method can efficiently solve the radiation problem for cylindrical arrays of thousands in number.

The work in this paper is divided into five sections. Section 1 is the introduction. Section 2 presents the formulation for truncated circular cylinders. Section 3 gives the approximate analytical solutions ignoring evanescent mode for the array of truncated cylinders. Section 4 provides the approximate calculation formula of the hydrodynamic coefficients of the array with a large number of cylinders. Section 5 is the conclusion of the paper.

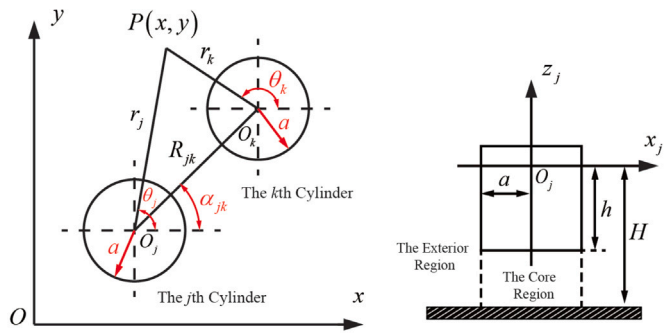

Fig. 1. Sketch of an array of truncated cylinders.

2. Formulation for truncated cylinders

2.1. The boundary value problem

When the trajectory length of wave water particle in a cycle is small compared with the characteristic size of the cylinder (i.e. Keulegan–Carpenter number is small, e.g. less than 2), the flow separation and friction can be ignored, and inertial force is dominant. In addition, considering the large ratio of cylinder diameter to wavelength (e.g. greater than 0.15), the diffraction effects should be considered. The wave steepness and cylinder motion are small, and the first-order theory is applicable. The present study is carried out under the above conditions. To sum up, the following assumptions are adopted: the fluid is incompressible, inviscid, the flow is unseparated and the motions of cylinders and waves are sufficiently small to linearize. In other words, this study is carried out within the framework of linear water wave theory. In benign sea state, the first-order hydrodynamic responses of floating body within this theoretical framework have been serving the field of offshore engineering with great success, and its applications are wide-spread. Obtaining the solution based on linearized theory is an essential step in the design of a new project. It is often sufficient for routine design and analysis in benign sea states, and can provide reference information for further nonlinear analysis and even extreme loads analysis in harsh sea states.

In the context of linear water wave theory, the five degrees of freedom motion (surge, sway, heave, roll, and pitch) of N uniformly rigid truncated cylinders of the same size is studied in this paper. Each cylinder in the array floats freely on the water surface. The mode of the yaw motion, which is axisymmetric about the cylinder, is ignored.

The schematic diagram of an array consists of N truncated cylinders is shown in Fig. 1(a). The array of truncated cylinders is located in the right-handed Cartesian coordinate system $Oxyz$, which is a global coordinate system. The xoy plane is located on the still-water level, and Oz is vertically upward. The jth cylinder is located in the local cylindrical coordinate system (r_j, θ_j, z_j), $j = 1, 2, 3, \ldots, N$. The origin O_j of the local cylindrical coordinate system is located at the center of the jth cylinder. The coordinate of the origin O_j of each cylinder in the Cartesian coordinate system $Oxyz$ is (x_j, y_j). The radius of each cylinder in the array is a. The distance and angle between the kth cylinder and jth cylinder are R_{jk} and α_{jk}, respectively. The coordinates of any point $P(x, y)$ in the field are (r_j, θ_j, z) in the jth local cylindrical coordinate system and (r_k, θ_k, z) in the kth local cylindrical coordinate system.

The vertical parameters of the array and the region division are illustrated by taking the jth cylinder as an example, as shown in Fig. 1(b). The water depth is H, which is assumed to be constant. The draft of the cylinder is h. The region is divided into two sub-regions: the exterior region ($a \le r \le \infty, 0 \le \theta \le 2\pi, -H \le z \le 0$) and the core region ($0 \le r \le a, 0 \le \theta \le 2\pi, -H \le z \le -h$).

It is assumed that the velocity potential and all the motion are time harmonic with angular frequency ω, therefore the velocity potential of the exterior region $\boldsymbol{\Phi}_{RD-E}(r, \theta, z, t)$ and the core region $\boldsymbol{\Phi}_{RD-C}(r, \theta, z, t)$ can be written as

$$\begin{aligned}\boldsymbol{\Phi}_{RD-E}(r, \theta, z, t) &= \mathrm{Re}\left[\phi_{RD-E}(r, \theta, z) \cdot e^{-\mathrm{i}\omega t}\right], \ \boldsymbol{\Phi}_{RD-C}(r, \theta, z, t) \\ &= \mathrm{Re}\left[\phi_{RD-C}(r, \theta, z) \cdot e^{-\mathrm{i}\omega t}\right], \end{aligned} \tag{1}$$

where Re is the real part of the parameter, ϕ_{RD-E} and ϕ_{RD-C} the spatial factors of the velocity potential of the core region and the exterior region, $\mathrm{i} = \sqrt{-1}$ the imaginary unit, t time.

The displacement of cylinder j in the sth mode is

$$\Xi_s^j(t) = \mathrm{Re}\left[\xi_s^j \cdot e^{-\mathrm{i}\omega t}\right], \tag{2}$$

where ξ_s^j is the spatial factors of the motion amplitude, $s = 1, 2, 3, 4, 5$ the modes of surge, sway, heave, roll, and pitch.

$\boldsymbol{\Phi}_{Rs-E}^j$ and $\boldsymbol{\Phi}_{Rs-C}^j$ denote the radiation velocity potential of cylinder j in the sth mode for the exterior region and the core region, respectively. Similar to the expression of Eq. (1), their spatial factors are ϕ_{Rs-E}^j and ϕ_{Rs-C}^j, respectively. The coordinate of the centroid of the cylinder is $(0, 0, \bar{z})$ when the cylinder is still floating on the water. The spatial factor ϕ_{Rs-E}^j of radiation potential of cylinder j in the sth mode for the exterior region satisfies the Laplace equation, the linear free surface condition, the impermeable condition on the body surface, the impermeable seabed condition and the Sommerfeld condition:

$$\nabla^2 \phi_{Rs-E}^j = 0, \ a \le r < \infty, \ -H \le z \le 0, \tag{3}$$

$$\frac{\partial \phi_{Rs-E}^j}{\partial z} - \frac{\omega^2}{g} \phi_{Rs-E}^j = 0, \ z = 0, \ a \le r < \infty, \tag{4}$$

$$\frac{\partial \phi_{Rs-E}^j}{\partial r} = \mathrm{i}\omega \xi_s^j \cdot \tilde{n}_s, \ r = a, \ -h \le z \le 0, \tag{5}$$

$$\frac{\partial \phi_{Rs-E}^j}{\partial z} = 0, \ z = -H, \ a \le r < \infty, \tag{6}$$

and

$$\lim_{r \to \infty} \sqrt{r} \left(\frac{\partial \phi_{Rs-E}^j}{\partial r} - \mathrm{i} k_0 \phi_{Rs-E}^j \right) = 0, \tag{7}$$

where k_0 is wavenumber, g is the acceleration of gravity, and

$$\tilde{n}_s = \left[n_1, n_2, n_3, y n_3 - (z - \bar{z}) n_2, (z - \bar{z}) n_1 - x n_3\right] \tag{8}$$

is the generalized normal vector of the object surface.

The spatial factor ϕ_{Rs-C}^j of radiation potential of cylinder j in the sth mode for the core region satisfies the Laplace equation, the impermeable condition on the body surface and the impermeable seabed condition:

$$\nabla^2 \phi_{Rs-C}^j = 0, \ 0 < r \le a, -H \le z \le -h, \tag{9}$$

$$\frac{\partial \phi_{Rs-C}^j}{\partial z} = -\mathrm{i}\omega \xi_s^j \cdot \tilde{n}_s, \ z = -h, \ 0 < r \le a, \tag{10}$$

$$\frac{\partial \phi_{Rs-C}^j}{\partial z} = 0, \ z = -H, \ 0 < r \le a. \tag{11}$$

The impermeable condition on the body surface, which is satisfied by ϕ_{Rs-E}^j and ϕ_{Rs-C}^j, can be further expressed as follows by replacing Eq. (8) into Eq. (5) and Eq. (10), respectively:

$$\frac{\partial \phi_{Rs-E}^j}{\partial r} = -\mathrm{i}\omega \xi_s^j \cdot f_s(z) \sum_{m=-\infty}^{\infty} \lambda_{ms} e^{\mathrm{i}m\theta}, \ r = a, \ -h \le z \le 0, \tag{12}$$

$$\frac{\partial \phi_{Rs-C}^j}{\partial z} = -\mathrm{i}\omega \xi_s^j \cdot \frac{\partial \Lambda_s(r, z)}{\partial z} \sum_{m=-\infty}^{\infty} \lambda_{ms} e^{\mathrm{i}m\theta}, \ z = -h, \ 0 < r \le a, \tag{13}$$

where

$$f_s(z)=\begin{cases}1, & s=1,\ 2\\ 0, & s=3\\ -(z-\bar{z}), & s=4\\ (z-\bar{z}), & s=5,\end{cases} \tag{14}$$

$$\Lambda_s(r,z)=\begin{cases}0, & p=1,\ 2\\ \frac{1}{2(H-h)}\left[(z+H)^2-\frac{r^2}{2}\right], & p=3\\ \frac{r}{2(H-h)}\left[(z+H)^2-\frac{r^2}{4}\right], & p=4\\ -\frac{r}{2(H-h)}\left[(z+H)^2-\frac{r^2}{4}\right], & p=5,\end{cases} \tag{15}$$

and

$$\lambda_{1s}=\begin{cases}\frac{1}{2}, & s=1,\ 5\\ 0, & s=3\\ \frac{1}{2\mathrm{i}}, & s=2,\ 4,\end{cases}\quad \lambda_{0s}=\begin{cases}0, & s=1,\ 5\\ 1, & s=3\\ 0, & s=2,\ 4,\end{cases}\quad \lambda_{-1s}=\begin{cases}\frac{1}{2}, & s=1,\ 5\\ 0, & s=3\\ -\frac{1}{2\mathrm{i}}, & s=2,\ 4,\end{cases}$$
$$\lambda_{ms}=0,\ m\neq 0,\ \pm 1 \tag{16}$$

At the boundary of the sub-regions, the spatial factors of velocity potential satisfy the appropriate transmission conditions:

$$\phi^j_{Rs-E}=\phi^j_{Rs-C},\ r=a,\ -H\le z\le -h, \tag{17}$$

$$\frac{\partial\phi^j_{Rs-E}}{\partial r}=\frac{\partial\phi^j_{Rs-C}}{\partial r},\ r=a,\ -H\le z\le -h. \tag{18}$$

According to Eqs. (3)–(18), ϕ^j_{Rs-E} and ϕ^j_{Rs-C} could be obtained, which are the basis of solving the hydrodynamic problems of the array of truncated cylinders.

2.2. The solutions for velocity potentials

The radiation velocity potential ϕ^j_{Rs-E} of cylinder j in the sth mode for the exterior region is

$$\phi^j_{Rs-E}=-\mathrm{i}\omega_0\xi^j_s\cdot\left(\mathbf{R}^j_s\right)^T\cdot\boldsymbol{\psi}^{D-E}_j, \tag{19}$$

where $\left(\mathbf{R}^j_s\right)^T$ is the radiative characteristic coefficient, which is a row vector. Each element $R^j_s(n,m)$ of the vector is as follows:

$$R^j_s(n,m)=\begin{cases}\frac{D_{m0s}\cosh(k_0H)}{H'^{(1)}_m(k_0a)\cdot N_0^{1/2}}, & n=0\\ \frac{D_{mns}}{K'_m(k_na)\cdot N_n^{1/2}}, & n\ge 1.\end{cases} \tag{20}$$

The solution of coefficient D_{mns} could be found at Zeng and Tang (2013), Zeng et al. (2016). $H^{(1)}_m=J_m+\mathrm{i}Y_m$ is the first kind of Hankel function of order m. J_m and Y_m are the first and second kind of Bessel function of order m, respectively. K_m is the first kind of modified Bessel function of order m. k_0 and k_n are wavenumbers, which are determined by the following dispersion relation:

$$k_0\tanh(k_0H)=\omega^2/g,\ k_n\tan(k_nH)=-\omega^2/g. \tag{21}$$

Expressions N_0 and N_n can be written as

$$N_0=\frac{1}{2}[1+\frac{\sinh(2k_0H)}{2k_0H}],\ N_n=\frac{1}{2}[1+\frac{\sin(2k_nH)}{2k_nH}].$$

Vector $\boldsymbol{\psi}^{D-E}_j$ represents partial diffraction wave in the exterior region. The expression of its element is as follows:

$$\psi^{D-E}_j(n,m)=\begin{cases}Y_0(z)H_m(k_0r_j)e^{\mathrm{i}m\theta_j}, & n=0\\ Y_n(z)K_m(k_nr_j)e^{\mathrm{i}m\theta_j}, & n\ge 1.\end{cases} \tag{22}$$

Expression Y_n is a vertical characteristic function, expressed as

$$Y_n(z)=\begin{cases}\frac{\cosh[k_0(z+H)]}{\cosh(k_0H)}, & n=0\\ \cos[k_n(z+H)], & n\ge 1.\end{cases} \tag{23}$$

Based on the Bessel addition theorem (Abramowitz and Stegun, 1964), Eq. (19) can be further written as follows:

$$\phi^j_{Rs-E}=-\mathrm{i}\omega_0\xi^j_s\cdot\left(\mathbf{R}^j_s\right)^T\cdot\mathbf{T}_{jk}\cdot\boldsymbol{\psi}^I_k, \tag{24}$$

where $\mathbf{T}_{jk}$ is the coordinate transformation matrix, expressed as

$$\mathbf{T}_{jk}(n,m,l)=\begin{cases}H_{m-l}(k_0R_{jk})e^{\mathrm{i}\alpha_{jk}(m-l)}, & n=0\\ K_{m-l}(k_nR_{jk})e^{\mathrm{i}\alpha_{jk}(m-l)}(-1)^l, & n\ge 1.\end{cases} \tag{25}$$

Vector $\boldsymbol{\psi}^I_k$ represents the partial incident wave. The expression of its element is as follows:

$$\psi^I_k(n,m)=\begin{cases}Y_0(z)J_m(k_0r_k)e^{\mathrm{i}m\theta_k}, & n=0\\ Y_n(z)I_m(k_nr_k)e^{\mathrm{i}m\theta_k}, & n\ge 1.\end{cases} \tag{26}$$

The diffraction potential of cylinder j as all the other cylinders oscillate in the sth mode is

$$\phi^j_{Ds-E}=\left(\mathbf{A}^j_s\right)^T\cdot\boldsymbol{\psi}^{D-E}_j=\left(\mathbf{A}^j_s\right)^T\cdot\mathbf{T}_{jk}\cdot\boldsymbol{\psi}^I_k, \tag{27}$$

where $\left(\mathbf{A}^j_s\right)^T$ is a row vector of the unknown coefficient of wave diffraction, and any element of it is A^j_{mns}.

Therefore, the total incident potential in the vicinity of cylinder k is the sum of the radiation potentials and the diffraction potentials caused by the other N-1 cylinders oscillate in the sth mode, as follows:

$$\phi^I_{Rk}=\sum_{j=1,j\neq k}^{N}\left[-\mathrm{i}\omega\xi^j_s\cdot\left(\mathbf{R}^j_s\right)^T+\left(\mathbf{A}^j_s\right)^T\right]\cdot\mathbf{T}_{jk}\cdot\boldsymbol{\psi}^I_k. \tag{28}$$

For cylinder k in the sth mode, the diffraction coefficients $\mathbf{A}^k_s$ and the total incident potential coefficients $\mathbf{A}^k_s=\mathbf{B}_k\cdot\sum_{j=1,j\neq k}^{N}\mathbf{T}^T_{jk}\cdot\left(-\mathrm{i}\omega_0\xi^j_s\cdot\mathbf{R}^j_s+\mathbf{A}^j_s\right)$ can be connected by the diffraction transfer matrix $\mathbf{B}^E_j$, which are given in the Appendix. Therefore, we obtain a system of linear equations to determine the unknown coefficients A^j_{mns}:

$$\mathbf{A}^k_s=\mathbf{B}_k\cdot\sum_{j=1,j\neq k}^{N}\mathbf{T}^T_{jk}\cdot\left(-\mathrm{i}\omega_0\xi^j_s\cdot\mathbf{R}^j_s+\mathbf{A}^j_s\right). \tag{29}$$

The Eq. (29) is truncated to an $Nn_0\left(2m_0+1\right)$-dimensional system of linear equations, where $n=0,\ 1,\ 2,\ldots,\ n_0-1$, $m=-m_0,\ldots,\ m_0$. In this case, if we have the oscillation amplitude ξ^j_s ($s=1,\ 2,\ 3,\ 4,\ 5$), we can obtain the diffraction coefficient vector $\mathbf{A}^j_s$ of the array for the exterior region. Then, the total radiation velocity potential in the vicinity of cylinder j in the sth mode for the exterior region can be written as

$$\phi^{js}_{RD-E}=\left[-\mathrm{i}\omega\xi^j_s\cdot\left(\mathbf{R}^j_s\right)^T+\left(\mathbf{A}^j_s\right)^T\right]\cdot\boldsymbol{\psi}^{D-E}_j+\sum_{i=1,i\neq j}^{N}\left[-\mathrm{i}\omega\xi^i_s\cdot\left(\mathbf{R}^i_s\right)^T+\left(\mathbf{A}^i_s\right)^T\right]\cdot\mathbf{T}_{ij}\cdot\boldsymbol{\psi}^I_j. \tag{30}$$

In all modes, the total radiation velocity potential in the vicinity of cylinder j can be written as

$$\phi^j_{RD-E}=\sum_{s=1}^{5}\phi^{js}_{RD-E}. \tag{31}$$

Similarly, the total radiation velocity potential in the vicinity of cylinder j can be written as

$$\phi^j_{RD-C}=\sum_{s=1}^{5}\left\{-\mathrm{i}\omega\xi^j_s\cdot\varphi^j_{Rs-C}+\sum_{i=1,i\neq j}^{N}\left[-\mathrm{i}\omega\xi^i_s\cdot\left(\mathbf{R}^i_s\right)^T+\left(\mathbf{A}^i_s\right)^T\right]\cdot\mathbf{T}_{ij}\cdot\left(\mathbf{B}^C_j\right)^T\cdot\boldsymbol{\psi}^{D-C}_j\right\}, \tag{32}$$

where φ^j_{Rs-C} is the radiation potential of cylinder j in the core region, $\mathbf{B}^C_j$ is the transfer matrix of cylinder j in the core region. See Appendix for details. The vector $\boldsymbol{\psi}^{D-C}_j$ is the partial-wave functions in the core region, and its elements are expressed as

$$\psi^{D-C}_j(n,m)=\begin{cases}r_j^{|m|}e^{\mathrm{i}m\theta_j}, & n=0\\ I_m\left(\frac{n\pi r_j}{H-h}\right)e^{\mathrm{i}m\theta_j}, & n\ge 1.\end{cases} \tag{33}$$

2.3. The hydrodynamic forces and moments

The dynamic pressure of fluid can be expressed as follows:

$$P\left(r_j,\theta_j,z,t\right)=\mathrm{Re}\left[p\left(r_j,\theta_j,z\right)\cdot e^{-\mathrm{i}\omega t}\right]. \tag{34}$$

where $p\left(r_j,\theta_j,z\right)$ is the spatial factor of dynamic pressure, which can be written as follows in the framework of linear water wave theory:

$$p\left(r_j,\theta_j,z\right)=\mathrm{i}\rho\omega\cdot\phi^{j}_{RD}(r_j,\theta_j,z), \tag{35}$$

where ρ is the density of the fluid, $\phi^{j}_{RD}(r_j,\theta_j,z)$ is the total radiation potential in the core (or the exterior) region.

The hydrodynamic forces and moments of cylinder j in the sth mode can be expressed as

$$\begin{cases} F^{j}_{s}=\iint_S p(r_j,\theta_j,z)\cdot\tilde{n}_s dS, & s=1,\ 2,\ 3 \\ M^{j}_{s}=\iint_S p(r_j,\theta_j,z)\cdot\tilde{n}_s dS, & s=4,\ 5 \end{cases}, \tag{36}$$

where $\tilde{n}_s$ is the generalized normal vector shown in Eq. (8). The relationship between the added mass $\mu_{s_1s_2}\ \left(s_1,\ s_2=1,\ 2,\ 3,\ 4,\ 5\right)$ and the damping coefficient $\lambda_{s_1s_2}\ \left(s_1,\ s_2=1,\ 2,\ 3,\ 4,\ 5\right)$ is as follows:

$$\rho\iint_S\phi^{js_2}_{RD}\left(r_j,\theta_j,z\right)\cdot\tilde{n}_{s_1}\mathrm{d}S=\mu_{s_1s_2}+\frac{\mathrm{i}\lambda_{s_1s_2}}{\omega}. \tag{37}$$

Where, The added mass $\mu_{s_1s_2}$ and damping coefficient $\lambda_{s_1s_2}$ are non-dimensionalized by $\rho\pi a^2h$ and $\rho\pi a^2h\omega$, respectively. Then, the added mass $\mu_{s_1s_2}$ and the damping coefficient $\lambda_{s_1s_2}$ are expressed as follows:

$$\begin{cases} \mu_{s_1s_2}=\mathrm{Re}\left[\rho\iint_S\phi^{js_2}_{RD}\left(r_j,\theta_j,z\right)\cdot\tilde{n}_{s_1}\mathrm{d}S\right] \\ \lambda_{s_1s_2}=\omega\,\mathrm{Im}\left[\rho\iint_S\phi^{js_2}_{RD}\left(r_j,\theta_j,z\right)\cdot\tilde{n}_{s_1}\mathrm{d}S\right] \end{cases}, \tag{38}$$

where $\mu_{s_1s_2}$ and $\lambda_{s_1s_2}$ represent the added mass and the damping coefficient in the s_1 direction of radiation velocity potential $\phi^{js_2}_{RD}\left(r_j,\theta_j,z\right)$ due to oscillation in the s_2th mode.

3. Approximate analytical solutions ignoring evanescent mode

By studying the interaction between floating cylinders and wave field, the hydrodynamic characteristics of each floating cylinder can be obtained, which is a theoretical foundation for the structural design, strength check and fatigue analysis of the floating structures. The key to evaluate the hydrodynamic characteristics of floating cylinders is to accurately calculate the interaction between them. The interaction between cylinders mainly includes two aspects: propagating mode and evanescent mode. When (Kagemoto and Yue, 1986)'s exact algebraic method is used to solve the hydrodynamic problems of floating cylinders, the existence of evanescent mode greatly increases the difficulty of solving. It is found that the influence of evanescent mode between cylinders on hydrodynamic characteristics can be ignored in some cases. Previous studies mainly focused on the case that the number of cylinders is small and the spacing between adjacent cylinders is large, but there is no research on the effect of evanescent mode in the case of small cylinder spacing. This paper focuses on the influence of evanescent mode of truncated cylinders array with small spacing on the hydrodynamic coefficients.

For Eqs. (24), (27), (28), (29), (30) and (32), $n=0$ in the coordinate transformation matrix $\mathbf{T}_{jk}$ represents the propagating mode, and $n\geqslant 1$ represents the evanescent modes. In some case, the coordinate transformation matrix $\mathbf{T}_{jk}$ can be reduced to the following by using the approximation method which ignores the influence of evanescent mode:

$$T_{jk}(n,m,l)=\begin{cases} H_{m-l}(k_0R_{jk})e^{\mathrm{i}\alpha_{jk}(m-l)}, & n=0 \\ 0, & n\geqslant 1 \end{cases}. \tag{39}$$

In this case, the dimension of matrix calculation will be reduced from $Nn_0\left(2m_0+1\right)$ to $N\left(2m_0+1\right)$, which reduces the memory and time required for program calculation.

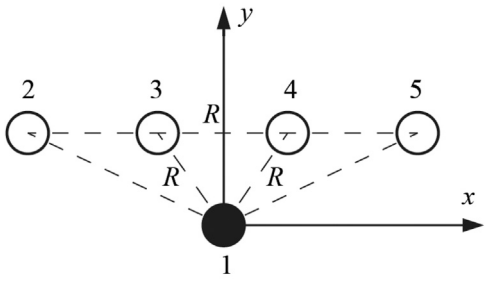

Fig. 2. Geometric configuration of the array with five truncated cylinders.

3.1. Effect of evanescent mode between cylinders on hydrodynamic coefficients

Here, an array of truncated cylinders as shown in Fig. 2 was investigated to study the effect of the evanescent mode between cylinders on hydrodynamic coefficients. The black solid circle and the hollow circle denote oscillating and fixed cylinders, respectively. The cylinder spacing is R. The ratio of the water depth and draft to the radius of the cylinder is $H/a=20$, and $h/a=10$, respectively. The ratio of cylinder spacing is taken as $R/a=2.4$, 3.0, and 5.0.

$\mu^{s_is_j}_{ij}\ \left(\lambda^{s_is_j}_{ij}\right)$ denote the added mass (damping) coefficient of cylinder i in the s_i direction due the oscillation of cylinder j in the s_j direction, where $s_i=1,2,3,4,5$. Kagemoto and Yue (1986)'s exact algebraic method and formula (39) without considering evanescent mode are applied respectively. Given the oscillation of cylinder 1, the added mass and damping coefficient of cylinder 1 and 4 under three kinds of cylinder spacing-radius ratios were investigated.

Fig. 3 shows the added mass and damping coefficient of cylinder 1 and 4 as cylinder 1 oscillates in sway mode with prescribed unit amplitude. The added mass and damping coefficient are non-dimensionalized by $\rho\pi a^2h$ and $\rho\pi a^2h\omega$, respectively. Fig. 4 shows the added mass and damping coefficient of the cylinder 1 and 4 as cylinder 1 oscillates in heave mode with prescribed unit amplitude. It can be seen from Fig. 3(a), (b) and Fig. 4(a), (b) that the evanescent mode has a great influence on the added mass, which cannot be ignored.

It can be found from Figs. 3(a) and 4(a) that the added mass which ignores the evanescent mode between cylinders tends to be a constant with the increase of dimensionless wavenumber. It can be concluded from the later discussion that this constant is actually the added mass caused by the radiation motion of a single cylinder. It can be found from Figs. 3(b) and 4(b) that the added mass, which ignores the evanescent mode, tends to zero with the increase of dimensionless wavenumber. This shows that the added mass of the fixed cylinder is almost caused by the evanescent mode between the cylinders. A good agreement between results of the exact algebraic method and the results of this paper which ignore the evanescent mode is observed from the comparison in Fig. 3(c), (d) and Fig. 4(c), (d). It can be concluded the damping coefficient is only affected by the propagating mode. In addition, when the wavenumber increases gradually, the damping coefficient caused by the propagating mode tends to zero.

According to the above analysis and numerical test results, even if the cylinder spacing is very small, the evanescent modes between cylinders have little effect on the damping coefficient, but have a great influence on the added mass. Therefore, the effect of evanescent mode can be ignored in the study of damping coefficient.

Next, we focus on the characteristics of the added mass in order to get a simplified and fast calculation method. Fig. 5(a) and (b) show the added mass caused by the evanescent mode under the corresponding conditions of Figs. 3 and 4, respectively. Obviously, with the increase of dimensionless wavenumber, the added mass caused by the evanescent mode tends to be constant. This phenomenon is not accidental and has been confirmed by a large number of numerical experiments on other arrangements and cylinder numbers. This property is the basis of the simplified formula for calculating the added mass.

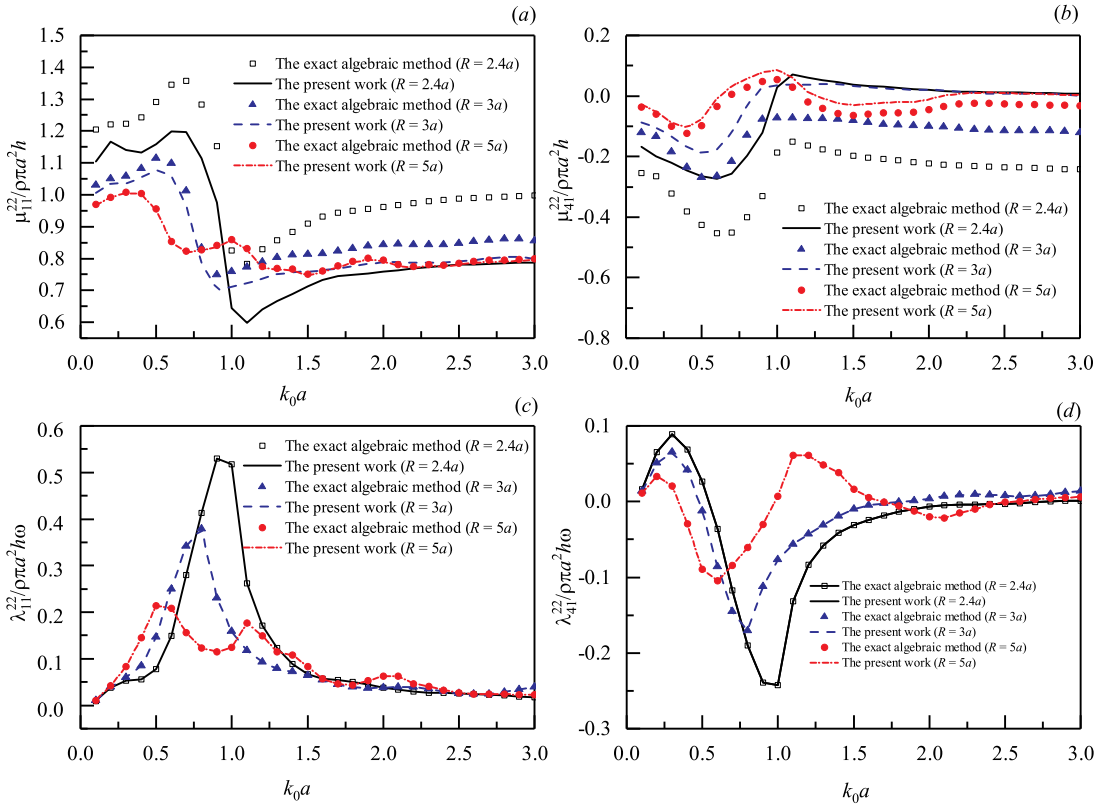

Fig. 3. Hydrodynamic coefficients of cylinder 1 and 4 as cylinder 1 oscillates in sway mode with prescribed unit amplitude. (*a*) cylinder 1: added mass. (*b*) cylinder 4: added mass. (*c*) cylinder 1: damping coefficient. (*d*) cylinder 4: damping coefficient.

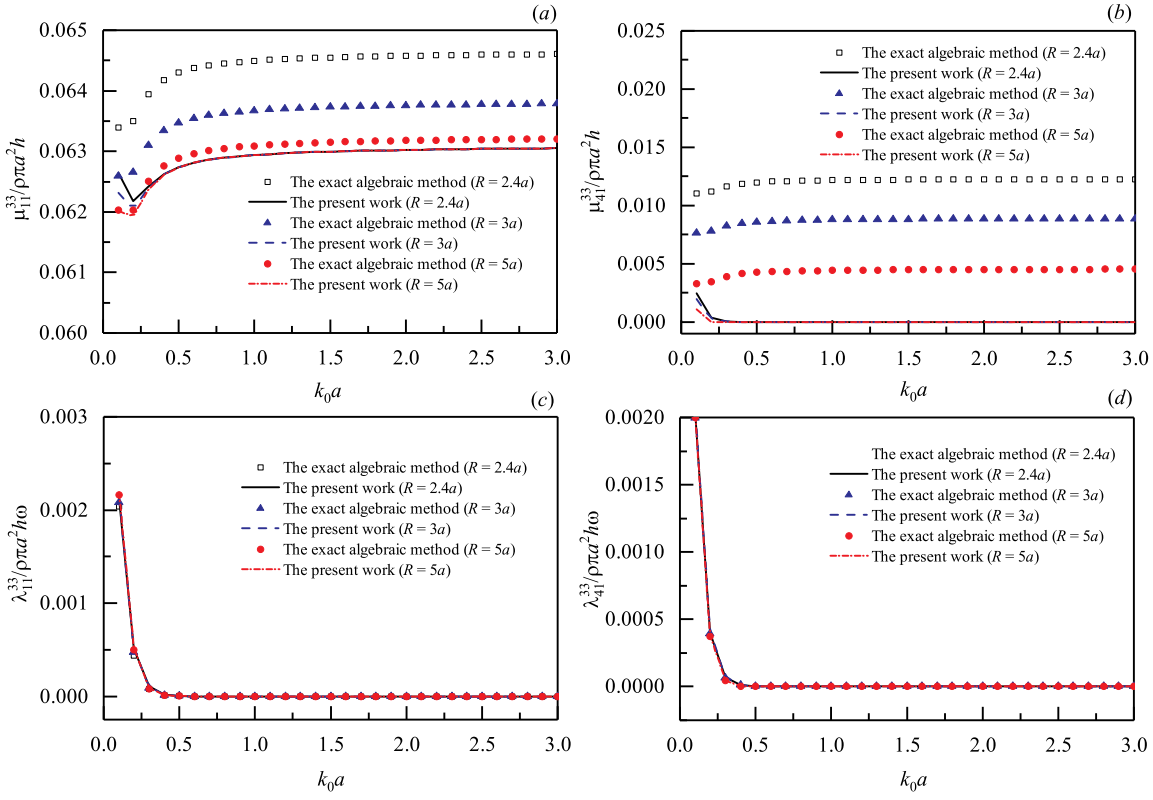

Fig. 4. Hydrodynamic coefficients of cylinder 1 and 4 as cylinder 1 oscillates in heave mode with prescribed unit amplitude. (*a*) cylinder 1: added mass. (*b*) cylinder 4: added mass. (*c*) cylinder 1: damping coefficient. (*d*) cylinder 4: damping coefficient.

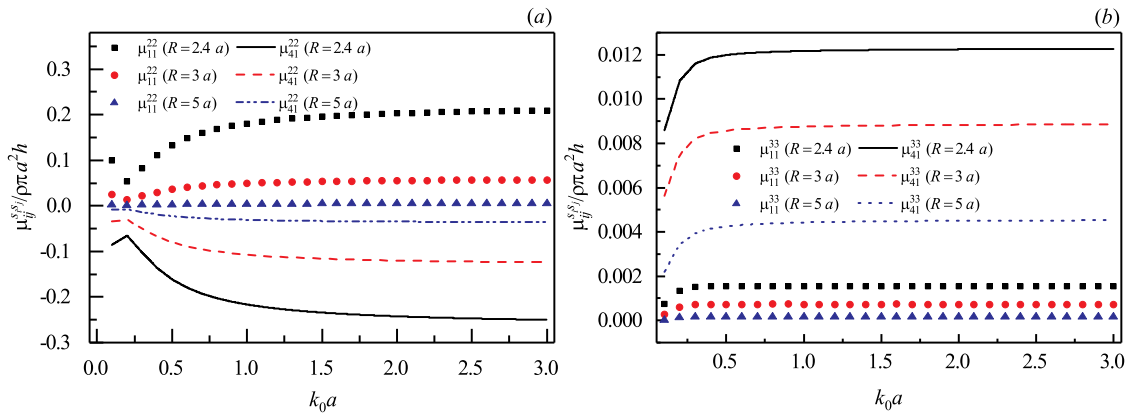

Fig. 5. The added mass of cylinder 1 and 4 caused by evanescent mode as cylinder 1 oscillates in sway mode (a) and heave mode (b) with prescribed unit amplitude.

3.2. Mechanism analysis of effect of evanescent mode between cylinders on hydrodynamic coefficients

In order to analyze the influence mechanism of evanescent mode between cylinders on hydrodynamic coefficients, the simplest truncated two-cylinders model is discussed in this paper. Both cylinders are located on the x-axis. Cylinder 1 oscillates in any mode with prescribed unit amplitude and cylinder 2 is fixed. The heave hydrodynamic coefficients μ_{11}^{33} (λ_{11}^{33}) of cylinder 1 caused by the heave motion with unit amplitude of itself are analyzed theoretically. In this case, the total radiation potential which causes the vertical hydrodynamic coefficient is determined by Eq. (32). Therefore, in the above example, the total radiation velocity potential in the vicinity of cylinder 1 for the core region is reduced from Eq. (32) to

$$\phi_{RD-C}^{1} = -\mathrm{i}\omega\varphi_{R3-C}^{1} + \left(\mathbf{A}_3^2\right)^T \cdot \mathbf{T}_{21} \cdot \left(\mathbf{B}_1^C\right)^T \cdot \boldsymbol{\psi}_1^{D-C}, \tag{40}$$

where φ_{R3-C}^{1} represents the radiation potential radiated by cylinder 1 for the core region, see Appendix. In Eq. (40), the first term represents the radiation velocity potential in the core region of cylinder 1 without considering the interaction between cylinders. The second term represents the velocity potential in the core region of cylinder 1 caused by the diffraction of cylinder 2, which includes two parts: propagating mode velocity potential and evanescent mode velocity potential. In Eq. (40), there is no radiation velocity potential of cylinder 2 because cylinder 2 is fixed and the oscillation amplitude is zero.

In this section, the total added mass (damping) coefficient (including evanescent mode) of cylinder 1 determined by Eq. (40), the added mass (damping) coefficient of isolated cylinder determined by the first term of Eq. (40), the added mass (damping) coefficient caused by the diffraction of cylinder 2, the added mass (damping) coefficient caused by propagating mode and evanescent mode of the diffraction of cylinder 2, are studied. The geometric dimensions of the two-cylinders model are $h = 0.4H$ and $R = 2.4a$. Fig. 6(a) shows the total added mass of cylinder 1 due to the oscillation of cylinder 1 in heave mode with prescribed unit amplitude. By contrast, Fig. 6(a) also shows the added mass in the case of cylinder 1 as an isolated cylinder. It can be seen that with the increase of dimensionless wavenumber, the curves gradually tend to a constant, corresponding to two asymptotes with values of 0.1585 and 0.1565 respectively. Fig. 6(b) shows the added mass of the heave of cylinder 1 caused by the diffraction effect of cylinder 2, and by the propagation (evanescent) diffraction effect of cylinder 2. It can be seen that when the dimensionless wavenumber is small, both the propagation and evanescent diffraction effect have a great influence on the heave added mass of cylinder 1.

With the increase of dimensionless wavenumber, the contribution of the propagating mode to the added mass becomes zero. The heave added mass of cylinder 1 caused by the diffraction effect of cylinder 2 is completely determined by the evanescent mode components. It can be seen that with the increase of dimensionless wavenumber, the added heave mass of cylinder 1 caused by the propagation diffraction effect of cylinder 2 tends to an asymptote with a value of 0, while that caused by the evanescent diffraction effect of cylinder 2 tends to an asymptote with the value of 0.00162. It can be seen from Fig. 6(a) and (b) that the heave added mass of cylinder 1 is mainly caused by its own heave motion, and the diffraction effect of cylinder 2 has little effect on this value. This is because there are only two cylinders. If the number of cylinders increases, the added mass caused by diffraction effect will be more significant. Similarly, corresponding to Fig. 6(a) and (b), Fig. 6(c) and (d) are the cases of damping coefficient. It can be seen from Fig. 6(c) that the total damping coefficient of cylinder 1 caused by the oscillation of cylinder 1 in heave mode with prescribed unit amplitude is almost identical with the added mass coefficient of cylinder 1 as an isolated cylinder. With the increase of the dimensionless wavenumber, the two curves rapidly decay and tend to zero. This means that the damping coefficient is almost all caused by the radiation effect of an isolated cylinder, and the influence of the diffraction effect of other cylinders on the damping coefficient is almost negligible. Fig. 6(d) confirms this conclusion.

Based on the theoretical analysis of the simplified model and the numerical experiments mentioned above, some preliminary conclusions can be obtained. The radiation effect of the isolated cylinder is the main factor for the added mass and damping coefficient. The added mass is sensitive to the existence of evanescent mode between cylinders, while the damping coefficient is not affected by the evanescent mode. The results show that the propagating mode has a significant effect on hydrodynamic coefficients only when the dimensionless wavenumber is small. With the increase of dimensionless wavenumber, the hydrodynamic coefficient caused by propagating mode tends to zero. The damping coefficient is only affected by the propagating mode in the radiation velocity potential, and is not sensitive to the evanescent mode between cylinders. The effect of evanescent mode on the added mass is great and cannot be ignored. When the dimensionless wavenumber is large, the added mass caused by the evanescent mode is constant, which is the basis of further analysis.

According to Eq. (29), the partial wave of the propagating mode and the partial wave of the evanescent mode are not independent, and the existence of the evanescent mode between cylinders will affect the added mass caused by the propagating mode. Therefore, it is necessary to study the influence of evanescent mode on propagating mode. Here, $\tilde{\mu}_2$ denotes the heave added mass of cylinder 1 caused by the diffraction partial wave of the evanescent mode of cylinder 2 when considering the evanescent mode between cylinders. $\tilde{\mu}_1$ refers to the heave added mass of the cylinder 1 caused by the diffraction partial wave of the propagating mode of cylinder 2 when the evanescent mode is ignored. Therefore, $\tilde{\mu}_0 - \tilde{\mu}_1$ means the influence of the existence of evanescent mode on the propagating mode. $\tilde{\mu}_{11}^{33}$ is used to represent the heave

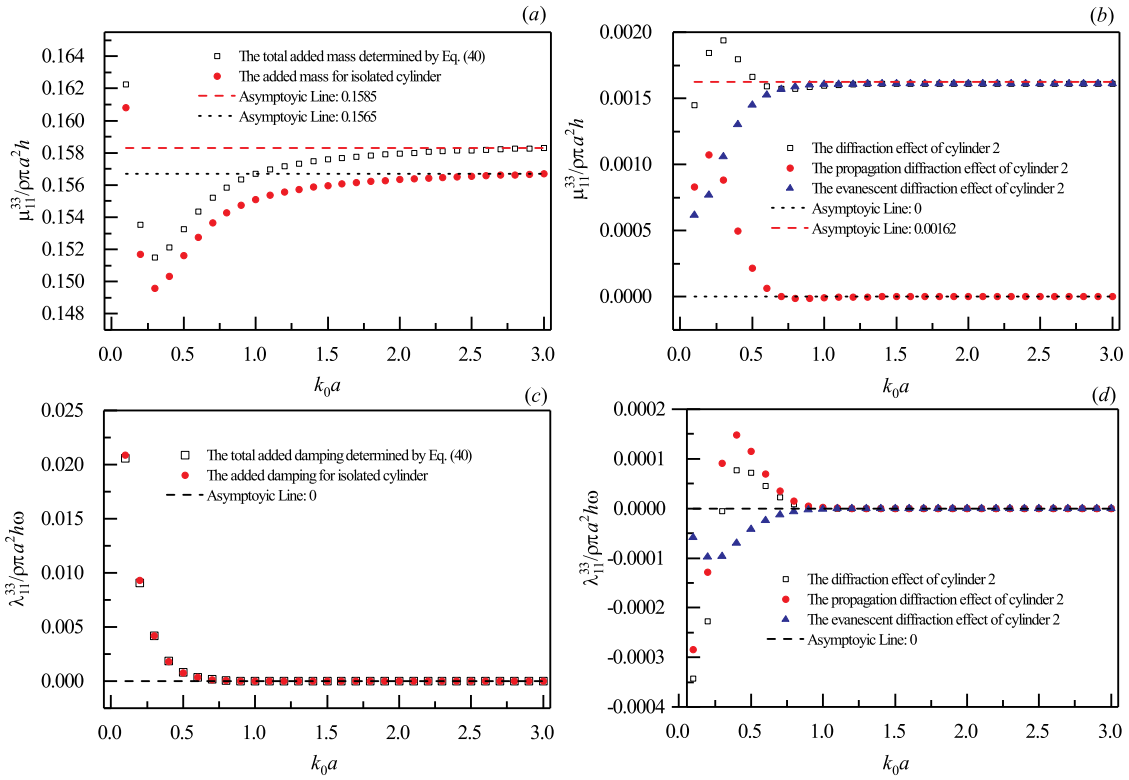

Fig. 6. Comparisons of hydrodynamic coefficients caused by different effect when the geometric dimensions are $h = 0.4H$ and $R = 2.4a$. (a) - (b): Added mass. (c) - (d): Damping coefficients.

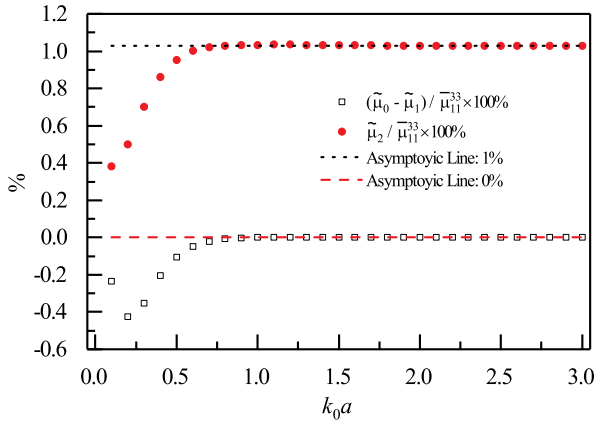

Fig. 7. Effect of evanescent mode between cylinders on added mass caused by the propagating mode.

added mass of cylinder 1 caused by the heave motion of cylinder 1 when the evanescent mode between cylinders is ignored.

As shown in Fig. 7, when the dimensionless wavenumber is more than 0.6, the curve of $(\tilde{\mu}_0 - \tilde{\mu}_1)/\bar{\mu}_{11}^{33} \times 100\%$ is constant to zero, and when the dimensionless wavenumber is less than 0.6, the influence order of magnitude is very small. This means that the existence of evanescent mode has little effect on the propagating mode. However, curve $\tilde{\mu}_2/\bar{\mu}_{11}^{33} \times 100\%$ is constant at 100% with the increase of dimensionless wavenumber. Combined with the previous analysis, when the wavenumber is large, the effect of the evanescent mode between cylinders on the added mass cannot be ignored. When the wavenumber is small, the added mass will be influenced by the propagating mode and the propagating mode change caused by the evanescent mode between the cylinders, but the influence will disappear when the wavenumber is large.

In the above analysis, the second term (diffraction partial item) in Eq. (32) is mainly discussed, excluding the amplitude term. The radiation partial item with amplitude also satisfies the conclusion, because they have the same form of propagating mode and evanescent mode as the second term of Eq. (32).

3.3. A fast formula for calculating the heave added mass caused by evanescent mode of two-cylinders

The results of the previous analysis and numerical experiments show that the evanescent mode between cylinders have great influence on the added mass, while the propagating mode between cylinders have little effect on the added mass (the effect is obvious only in the range of small wavenumber). Especially, for the heave motion mode, the effect of the propagating mode on the added mass has disappeared when the dimensionless wavenumber is greater than 0.4, and the added mass caused by the evanescent mode between cylinders tends to be a constant with the increase of the dimensionless wavenumber. Here, the truncated two-cylinders model in Section 3.2 is still discussed. Based on the theoretical analysis and the simplified numerical fitting method, a fast formula for calculating the added mass of the oscillating cylinder (cylinder 1) caused by evanescent mode between cylinders is given.

For the purpose of obtaining the variation law of $\tilde{\mu}_2$, a large number of results of various parameters such as draft-depth ratio h/H, cylinder spacing-radius ratio R/a, depth-radius ratio H/a and dimensionless wavenumber $k_0 a$ are calculated. Some meaningful conclusions are obtained. As a typical example, this section only gives the results of $H/a = 10$, other results are similar. Note that $\tilde{\mu}_2$ is non-dimensionalized by the heave added mass of the isolated cylinder with the same geometric configuration.

Fig. 8(a) shows the curve of the heave added mass (caused by the evanescent mode between cylinders) of the oscillating cylinder (cylinder 1) versus as the geometric parameters are $h/H = 0.4$ and $H/a = 10$. It can be seen from Fig. 8(a) that with the increase of dimensionless

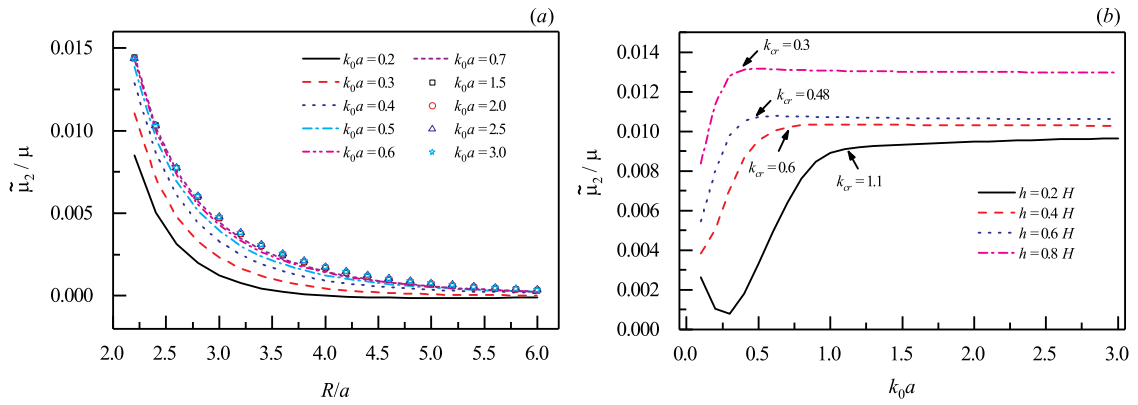

Fig. 8. Heave add mass (caused by the evanescent mode between cylinders) of the oscillating cylinder (cylinder 1) versus R/a (*a*) and k_0a (*b*) as the geometric parameters are $h/H = 0.4$ and $H/a = 10$.

wavenumber, the added mass caused by evanescent mode between cylinders gradually increases, but the increasing rate slows down, and all the curves tend to coincide. This means that when the wavenumber k_0a increases to a certain critical value k_{cr}, the added mass generated by the evanescent mode between cylinders will not increase with the increase of wavenumber, but will be a constant value.

Fig. 8(*b*) shows the curve of the heave added mass (caused by the evanescent mode between cylinders) of the oscillating cylinder (cylinder 1) versus dimensionless wavenumber as the geometric parameters are $h/H = 0.4$ and $H/a = 10$. It can be seen from Fig. 8(*b*) that the larger the draft-depth ratio h/H, the smaller the critical wavenumber k_{cr}. As can be seen from Fig. 8(*b*), when $h/H = 0.2, 0.4, 0.6, 0.8$, the value of k_{cr} are 1.1, 0.6, 0.48 and 0.3 respectively. This means that the larger the draft, the larger the range of dimensionless wavenumber with constant heave added mass. In addition, it can be seen from 8(*a*) that the added mass due to the evanescent mode between cylinders rapidly decreases with the increase of cylinder spacing. Especially for the curve with dimensionless wavenumber greater than critical wavenumber, it has the form of exponential decay, which provides the analysis direction for the analysis of attenuation mode.

According to Eq. (29), the diffraction coefficient obtained by substituting Eq. (39) into Eq. (29) is the diffraction coefficient that ignores the evanescent mode between cylinders, and its elements are represented by symbols $\bar{A}^j_{mns}$. The diffraction coefficient obtained by substituting Eq. (25) into Eq. (29) is the diffraction coefficient that considers the evanescent mode between cylinders, and its elements are represented by symbols A^j_{mns}. According to Eq. (32), for the truncated two-cylinders discussed in this section, when cylinder 1 oscillates in the heave mode with unit amplitude, the velocity potential $\tilde{\phi}^1_{RD-C}$ in the core region of cylinder 1 caused by the evanescent mode of cylinder 2 is expressed as

$$\tilde{\phi}^1_{RD-C} = \sum_{m=-\infty}^{\infty}\sum_{n=0}^{\infty}\sum_{l=-\infty}^{\infty}\left(A^2_{l03}-\bar{A}^2_{l03}\right)H^{(1)}_{l-m}\left(k_0R\right)B^C_2\left(n,0,m\right)\psi^{D-C}_2\left(n,m\right) + \sum_{p=1}^{\infty}\sum_{m=-\infty}^{\infty}\sum_{n=0}^{\infty}\sum_{l=-\infty}^{\infty}A^2_{lp3}K_{l-m}\left(k_pR\right)B^C_2\left(n,p,m\right)\psi^{D-C}_2\left(n,m\right) \tag{41}$$

Here, R is the cylinder spacing. The first term in Eq. (41) represents the effect of the existence of evanescent mode between cylinders on the propagating mode. It is a component of the velocity potential described in Section 3.2, which is a small quantity and can be ignored. Therefore, Eq. (41) can be further simplified as

$$\tilde{\phi}^1_{RD-C} \approx \sum_{p=1}^{\infty}\sum_{m=-\infty}^{\infty}\sum_{n=0}^{\infty}\sum_{l=-\infty}^{\infty}A^2_{lp3}K_{l-m}\left(k_pR\right)B^C_2\left(n,p,m\right)\psi^{D-C}_2\left(n,m\right). \tag{42}$$

The unknown coefficient A^2_{lp3} is the solution of the system of linear Eqs. (29). The diagonal elements of the coefficient matrix of the system of linear Eqs. (29) are 1. The elements of the off-diagonal and the right column vector are both small quantities. Assuming that the elements of the off-diagonal and the right column vector in the coefficient matrix are first-order small quantities, Eq. (29) is expanded by applying cram's rule, and the second-order small quantities are retained:

$$A^2_{lp3} = \frac{-\mathrm{i}\omega B^C_2\left(p,0,l\right)H_{-l}\left(k_0R\right)R^2_3\left(0,0\right)}{1-\sum_{l=-\infty}^{\infty}\sum_{m=-\infty}^{\infty}B^C_1\left(0,0,l\right)H_{m-l}\left(k_0R\right)B^C_2\left(0,0,m\right)H_{l-m}\left(k_0R\right)} + O\left(\varepsilon^3\right), \tag{43}$$

where $R^2_3(0,0)$ is the radiation characteristic coefficient determined by Eq. (20). By substituting Eq. (43) into Eq. (42), and substituting the asymptotic expression of the first kind of Hankel function and the second kind of modified Bessel function into Eq. (42) when $k_0R \to \infty$, it can be found that the two functions e^{-k_nR} and $1/R$ related to the cylinder spacing have the same form as the velocity potential $\tilde{\phi}^1_{RD-C}$. Therefore, the heave added mass of cylinder 1 generated by the velocity potential should have the following form:

$$\frac{\tilde{\mu}_2}{\mu} = \frac{1}{c\left(h/H, H/a\right)\cdot\left(\frac{R}{a}\right)^{m(h/H,H/a)}}\sum_{n=1}^{\infty}e^{-k_nR}, \tag{44}$$

where m and c are the functions of draft-depth ratio h/H and depth-radius ratio H/a, respectively. Function m controls the change rate of $\tilde{\mu}_2$ with cylinder spacing, and function c controls the amplitude of $\tilde{\mu}_2$. Through a large number of numerical experimental data, the function m is fitted by a bivariate quartic polynomial. The fitting expression of the function is as follows:

$$\begin{aligned} m\left(h/H, H/a\right) = {} & 9.14 - 0.249\frac{H}{a} - 28.08\frac{h}{H} + 0.12\left(\frac{H}{a}\right)\left(\frac{h}{H}\right) \\ & + 6.77\times10^{-3}\left(\frac{H}{a}\right)^2 \\ & + 56.0\left(\frac{h}{H}\right)^2 - 1.59\times10^{-4}\left(\frac{H}{a}\right)^3 + 5.35\times10^{-3}\left(\frac{H}{a}\right)^2\left(\frac{h}{H}\right) \\ & + 0.143\left(\frac{H}{a}\right)\left(\frac{h}{H}\right)^2 \\ & - 59.9\left(\frac{h}{H}\right)^3 + 1.85\times10^{-6}\left(\frac{H}{a}\right)^4 - 0.297\left(\frac{H}{a}\right)\left(\frac{h}{H}\right)^3 \\ & + 1.67\times10^{-3}\left(\frac{H}{a}\right)^2\left(\frac{h}{H}\right)^2 \\ & - 1.22\times10^{-4}\left(\frac{H}{a}\right)^3\left(\frac{h}{H}\right) + 26.6\left(\frac{h}{H}\right)^4 \end{aligned} \tag{45}$$

Once the expression of function m is obtained, the value of function c can be obtained. The fitting accuracy of function c depends on function m, the query table of function c under various conditions is shown in the Appendix.

Fig. 9 shows the comparison between the theoretical value of the heave added mass $\tilde{\mu}_2/\mu$ of cylinder 1 caused by the diffraction partial wave of the evanescent mode of cylinder 2 and the calculation

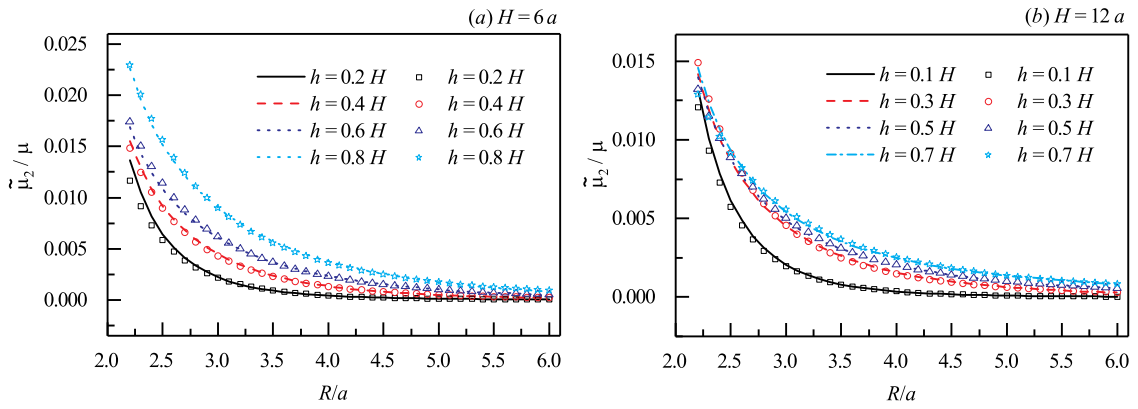

Fig. 9. Comparisons of the theoretical value of the heave added mass $\tilde{\mu}_2/\mu$ and calculation value of Eq. (44).

value of the fast calculation formula of Eq. (44) when considering the evanescent mode. The abscissa of the curve is the cylinder spacing-radius ratio R/a, the curve in the figure is the theoretical calculation value, and the scatter point is the calculation value of formula (44). Fig. 9(a) shows the case of depth-radius ratio $H/a = 6$ and draft-depth ratio $h/H = 0.2, 0.4, 0.6, 0.8$; Fig. 9(b) shows the case of depth-radius ratio $H/a = 12$ and draft-depth ratio $h/H = 0.1, 0.3, 0.5, 0.7$. It can be seen that Eq. (44) can accurately predict the added mass of the oscillating cylinder caused by the evanescent mode of the truncated two-cylinders model mentioned above, which provides a basis for predicting the hydrodynamic coefficients of the array with a large number of cylinders.

4. Approximate calculation formula of the hydrodynamic coefficients of the array with a large number of cylinders

The added mass of the oscillating cylinder (cylinder 1) caused by the evanescent mode in the two-cylinders model is given in Section 3.3, which can be used to simplify the calculation of the hydrodynamic coefficients of the array with a large number of cylinders. However, the support cylinder array of the offshore structure is mainly arranged in a single row, two rows, 2 × 2, rectangle, and so on. In this section, the fast calculation formula of the truncated two-cylinders model has modified appropriately and applied to an rectangular array with a large number of truncated cylinders. In order to illustrate the problem, this section takes the depth-radius ratio $H/a = 10$ as an example and gives a fast formula for calculating the added mass caused by the evanescent mode between cylinders when a cylinder oscillates. The arrangement of the rectangular array is shown in Fig. 10(a).

According to the different positions of the oscillating cylinder, rectangular arrays are divided into three types. Case A: the oscillating cylinder is located inside the rectangular array, as shown in Fig. 10(b). The black cylinder in Fig. 10(a) is such an oscillating cylinder. Case B: the oscillating cylinder is located on the edge of the rectangular array, as shown in Fig. 10(c). The white cylinder in Fig. 10(a) is such an oscillating cylinder. Case C: the oscillating column is located at the four corners of the rectangular array, as shown in Fig. 10(d). The gray cylinder in Fig. 10(a) is such an oscillating cylinder. It should be noted that the black cylinder in Fig. 10(b, c, d) represents the oscillating cylinder, and the form of Fig. 10(b, c, d) is the three most simplified forms of the rectangular array, similar to the "cell" of the rectangular array.

If we take the depth-radius ratio $H/a = 10$ as an example, then m and c in formula (45) can be simplified as follows:

$$\begin{cases} m = 1.31 + 5.66 \times 0.019^{h/d} \\ c = 4.73 - 48.93\frac{h}{d} + 264.0\left(\frac{h}{d}\right)^2 - 215.0\left(\frac{h}{d}\right)^3 \end{cases} . \tag{46}$$

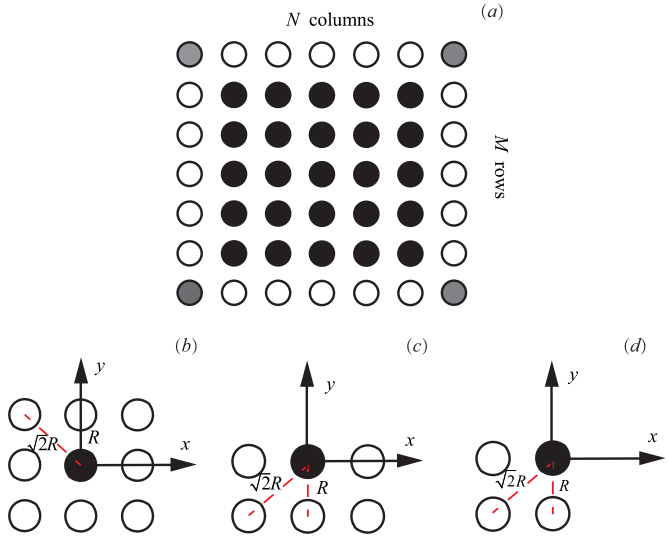

Fig. 10. Sketch of a rectangular array of truncated cylinders.

4.1. Effect of evanescent mode between cylinders on the added mass of the oscillating cylinder in the array of case A

Fig. 11 shows the heave added mass of oscillating cylinder caused by evanescent mode between cylinders in array of case A. The oscillating cylinder is located in the center of the array, and it heaves with unit amplitude. The geometric parameters of the model are $R = 2.4a$ and $h/H = 0.4$. The array arrangement is as follow: $3 \times 3, 5 \times 5, 7 \times 7, 9 \times 9$.

In Fig. 11, the vertical coordinate is the percentage of the additional mass difference of the central oscillation cylinder to the result of the isolated single oscillation cylinder when considering and ignoring the evanescent mode between cylinders modes. With the increase of the number of cylinders surrounding the oscillating cylinder, the added mass caused by the evanescent mode between cylinders increases gradually, but the increase range is smaller and smaller. In particular, the calculated results of 7 × 7 and 9 × 9 arrangement almost coincide. Therefore, for the array of case A, only the inner three-layers cylinder surrounding the oscillating cylinders has an effect on the added mass of the oscillating cylinder, and the influence of other peripheral cylinders can be ignored.

The influence of the evanescent mode between cylinders in the array of case A mainly comes from the innermost cylinder. Therefore, this section focus on the simplest 3 × 3 rectangular array model. The distance between the innermost cylinder and the central oscillating cylinder is R or $\sqrt{2}R$. In these two cases, the effect of evanescent mode

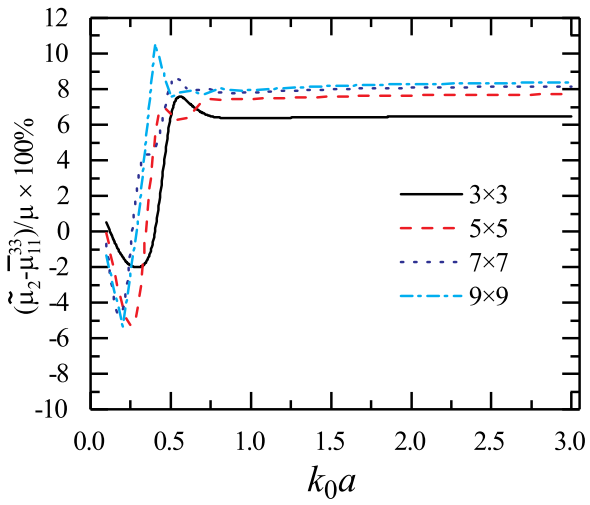

Fig. 11. Effect of evanescent mode between cylinders on added mass of oscillating cylinder with different array arrangement: $3\times3, 5\times5, 7\times7, 9\times9$.

on the added mass of the central oscillating cylinder can be compared with the truncated two-cylinders model in Section 3. The added mass of the central oscillating cylinder caused by the evanescent mode between cylinders of the whole array can be expressed as follows:

$$\frac{\tilde{\mu}_2}{\mu} = 4\left(\frac{C_1}{c\,(h/d)\cdot\left(\frac{R}{a}\right)^{m(h/d)}}\sum_{n=1}^{\infty}\mathrm{e}^{-k_nR} + \frac{C_2}{c\,(h/d)\cdot\left(\frac{\sqrt{2}R}{a}\right)^{m(h/d)}}\sum_{n=1}^{\infty}\mathrm{e}^{-k_n\sqrt{2}R}\right) + C_3. \tag{47}$$

Here, function m and c refer to formula (46). C_1 and C_2 are the correction coefficient for the cylinder whose distance from the central oscillating cylinder are R and $\sqrt{2}R$, respectively. They reflect the influence of array arrangement. C_3 reflects the influence of the outer cylinder, which is small.

A large number of numerical tests give the spectra of C_1, C_2 and C_3, as shown in Fig. 12. In practical engineering calculation, the value of correlation coefficient can be obtained through this graph. Fig. 11(a,b) shows the correction coefficient map of the simplest 3×3 rectangular array. Since only the innermost cylinder exists, C_3 is zero. Fig. 11(c,d,e) and Fig. 11(f,g,h) show the correction coefficient map of 5×5 and 7×7 rectangular array, respectively. When the row number M and column number N are greater than 7 (such as 8×8, 9×9, etc.), the correction coefficient of 7×7 arrangement can be directly adopted.

4.2. Effect of evanescent mode between cylinders on the added mass of oscillating cylinder in the array of case B

The simplified model of case B is 2×3 rectangular array, as shown in Fig. 10(c). Similar to the method in Section 4.1, based on the most simplified 2×3 rectangular array, the fast calculation formula is given. The influence of other cylinders is reflected in the correction coefficient.

As shown in Fig. 10(c), the black oscillating cylinder is in heave motion of unit amplitude, and the other cylinders are fixed. The added mass $\tilde{\mu}_2$ of the oscillating cylinder caused by the evanescent mode between cylinders in the array of case B can be expressed as follows:

$$\frac{\tilde{\mu}_2}{\mu} = 2\left(\frac{D_1}{c\,(h/d)\cdot\left(\frac{R}{a}\right)^{m(h/d)}}\sum_{n=1}^{\infty}\mathrm{e}^{-k_nR} + \frac{D_2}{c\,(h/d)\cdot\left(\frac{\sqrt{2}R}{a}\right)^{m(h/d)}}\sum_{n=1}^{\infty}\mathrm{e}^{-k_n\sqrt{2}R}\right) + \frac{D_3}{c\,(h/d)\cdot\left(\frac{R}{a}\right)^{m(h/d)}}\sum_{n=1}^{\infty}\mathrm{e}^{-k_nR} + D_4. \tag{48}$$

Here, function m and c refer to formula (46). D_1, D_2 and D_3 reflect the influence of array arrangement. D_4 reflects the effect of all cylinders except the innermost layer, which is small. D_1 is the correction coefficient corresponding to the left and right cylinders of the oscillating column in Fig. 10(c). D_2 is the correction coefficient for the cylinder whose distance from the central oscillating cylinder is $\sqrt{2}R$. D_3 is the correction coefficient corresponding to the cylinder above the oscillating cylinder in Fig. 10(c).

A large number of numerical tests give the spectra of D_1, D_2, D_3 and D_4, as shown in Fig. 13. In practical engineering calculation, the value of correlation coefficient can be obtained through this graph. Fig. 13(a,b,c) shows the correction coefficient map of the simplest 2×3 rectangular array. Since only the innermost cylinder exists, D_3 is zero. Fig. 13(d,e,f,g) and Fig. 13(h,l,j,k) show the correction coefficient map of 3×5 and 4×7 rectangular array, respectively. When the size of the rectangular array is greater than 4×7 (such as 5×8, 6×9, etc.), the correction coefficient of 4×7 arrangement can be directly adopted.

4.3. Effect of evanescent mode between cylinders on the added mass of oscillating cylinder in the array of case C

The simplified model of case C is 2×1 rectangular array, as shown in Fig. 10(d). Similar to the method in Sections 4.1 and 4.2, based on the most simplified 2×2 rectangular array, the fast calculation formula is given. The influence of other cylinders is reflected in the correction coefficient.

As shown in Fig. 10(d), the oscillating cylinder at the corner of the rectangular array is in heave motion of unit amplitude, and the other cylinders are fixed. The added mass $\tilde{\mu}_2$ of the oscillating cylinder caused by the evanescent mode between cylinders in the array of case C can be expressed as follows:

$$\frac{\tilde{\mu}_2}{\mu} = \frac{2F_1}{c\,(h/d)\cdot\left(\frac{R}{a}\right)^{m(h/d)}}\sum_{n=1}^{\infty}\mathrm{e}^{-k_nR} + \frac{F_2}{c\,(h/d)\cdot\left(\frac{\sqrt{2}R}{a}\right)^{m(h/d)}}\sum_{n=1}^{\infty}\mathrm{e}^{-k_n\sqrt{2}R} + F_3. \tag{49}$$

Here, function m and c refer to formula (46). F_1 and F_2 reflect the influence of array arrangement. F_3 reflects the effect of all cylinders except the innermost layer, which is small. F_1 and F_2 are the correction coefficient for the cylinder whose distance from the central oscillating column are R and $\sqrt{2}R$, respectively.

A large number of numerical tests give the spectra of F_1, F_2 and F_3, as shown in Fig. 14. In practical engineering calculation, the value of correlation coefficient can be obtained through this graph. Fig. 14(a,b) shows the correction coefficient map of the simplest 2×2 rectangular array. Since only the innermost cylinder exists, F_3 is zero. Fig. 14(c,d,e) and Fig. 14$(f,g,h,)$ show the correction coefficient map of 3×3 and 4×4 rectangular array, respectively. When the row number M and column number N are greater than 4 (such as 5×5, 6×6, etc.), the correction coefficient of 4×4 arrangement can be directly adopted.

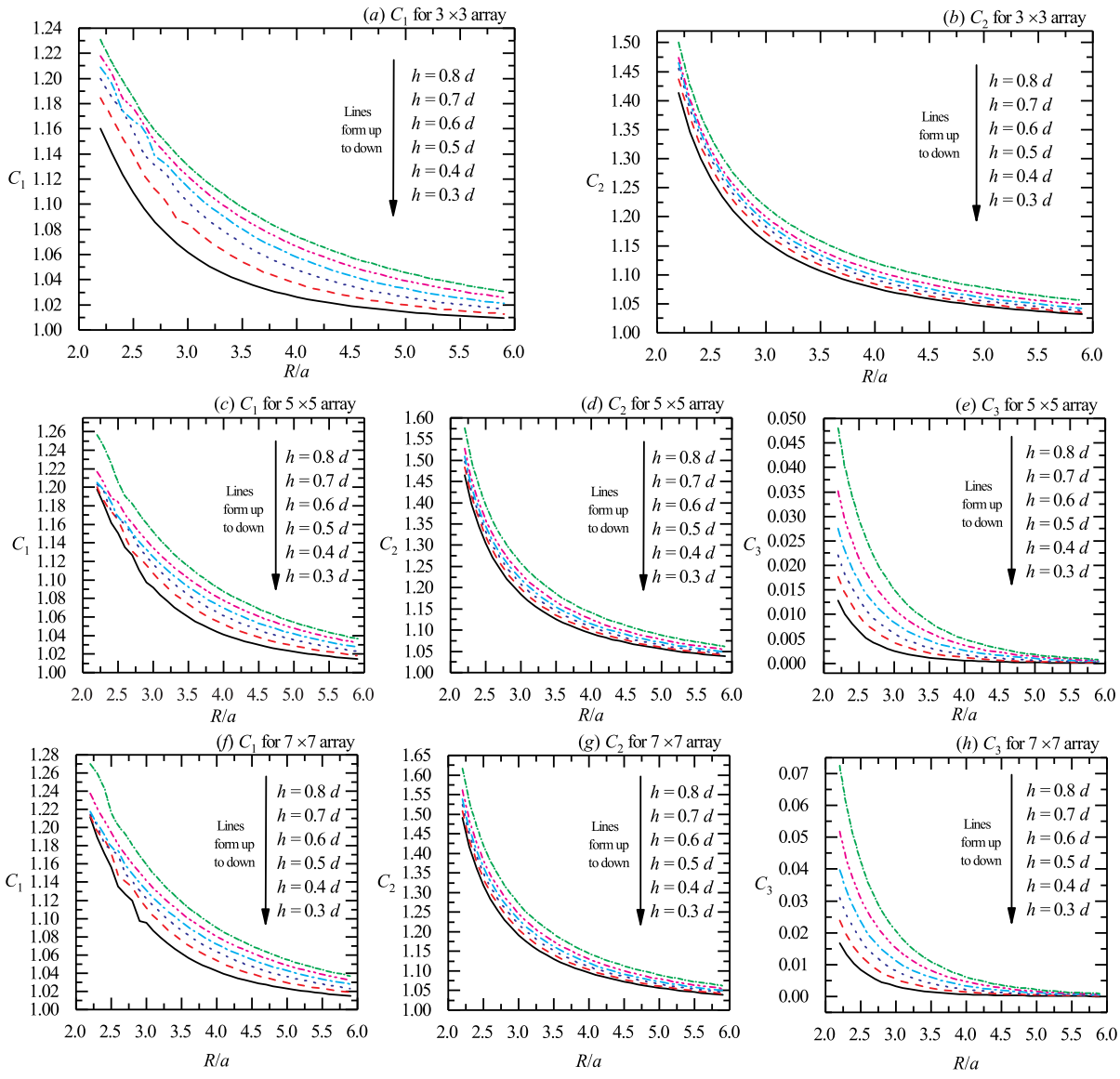

Fig. 12. Spectra of C_1, C_2 and C_3.

4.4. A fast hydrodynamic calculation method of the rectangular array with a large number of cylinders

Based on the truncated two-cylinders model, the rectangular array with a large number of cylinders are divided into three types (case A, B, C). A fast formula for calculating the added mass of an oscillating cylinder of the array caused by evanescent mode between cylinders is given. But this is only part of the result we need. So, how to get the hydrodynamic coefficients of the rectangular array with a large number of cylinders according to this fast calculation formula? The case of only one cylinder oscillating in an array is first considered. According to the previous discussion, the results of the damping coefficient are not affected by the evanescent mode between cylinders. Therefore, the influence of evanescent mode between cylinders on the damping coefficient can be ignored. In this way, the storage can be reduced to $1/N$ and the calculation time is greatly reduced, too. The added mass is significantly affected by the evanescent mode between cylinders, so it cannot be ignored. In this paper, the effect of evanescent mode between cylinders on the added mass of an oscillating cylinder is investigated. Based on the above discussion, the analysis of this paper is also applicable to non-oscillating cylinders, whose total added mass is only missing the part of the added mass of an isolated cylinder under the same amplitude motion compared to oscillating columns. For the oscillating cylinder, the added mass caused by the radiation motion of a isolated cylinder is calculated first, and then the added mass caused by the components of evanescent mode is calculated by using the fast calculation formulas such as Eqs. (47), (48) and (49). The algebraic sum of the two is the total added mass of the cylinder. The above is a fast method for solving the added mass of a single oscillating cylinder in a rectangular arrangement under a single mode. For an array of cylinders with multi-modal radiation motion, the linear superposition principle can be used to decompose into multiple single cylinder oscillation models to solve the problem, and the final result can be obtained by linear superposition.

The above approximate solution method may not be significant (or even cumbersome) for the hydrodynamic calculation of an array with a dozen or even dozens of truncated cylinders. The method avoids solving large-scale linear equations, so it is of great significance for the rapid calculation of an array with a large number of cylinders.

5. Conclusions

In this paper, based on the linear water wave theory, the hydrodynamic solution of truncated cylinder array with relative motion

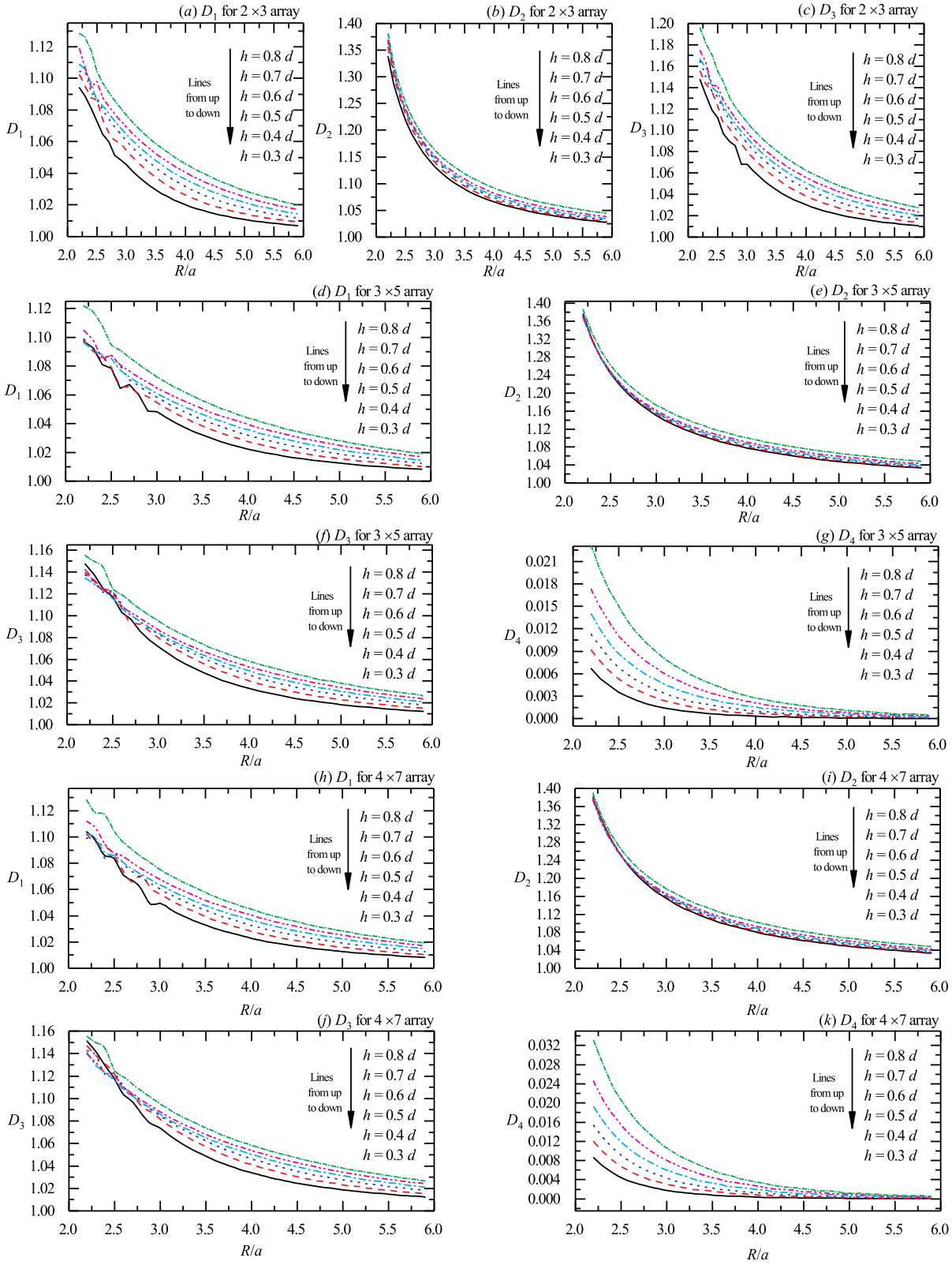

Fig. 13. Spectra of D_1, D_2, D_3 and D_4.

between cylinders is presented. The analytical expressions of velocity potential, hydrodynamic force and moment are given. The influence of the evanescent mode between cylinders on the hydrodynamic characteristics of the array of cylinders is studied. The conventional hydrodynamic solution of an array with a large number of truncated cylinders takes up a lot of computational memory and takes a long

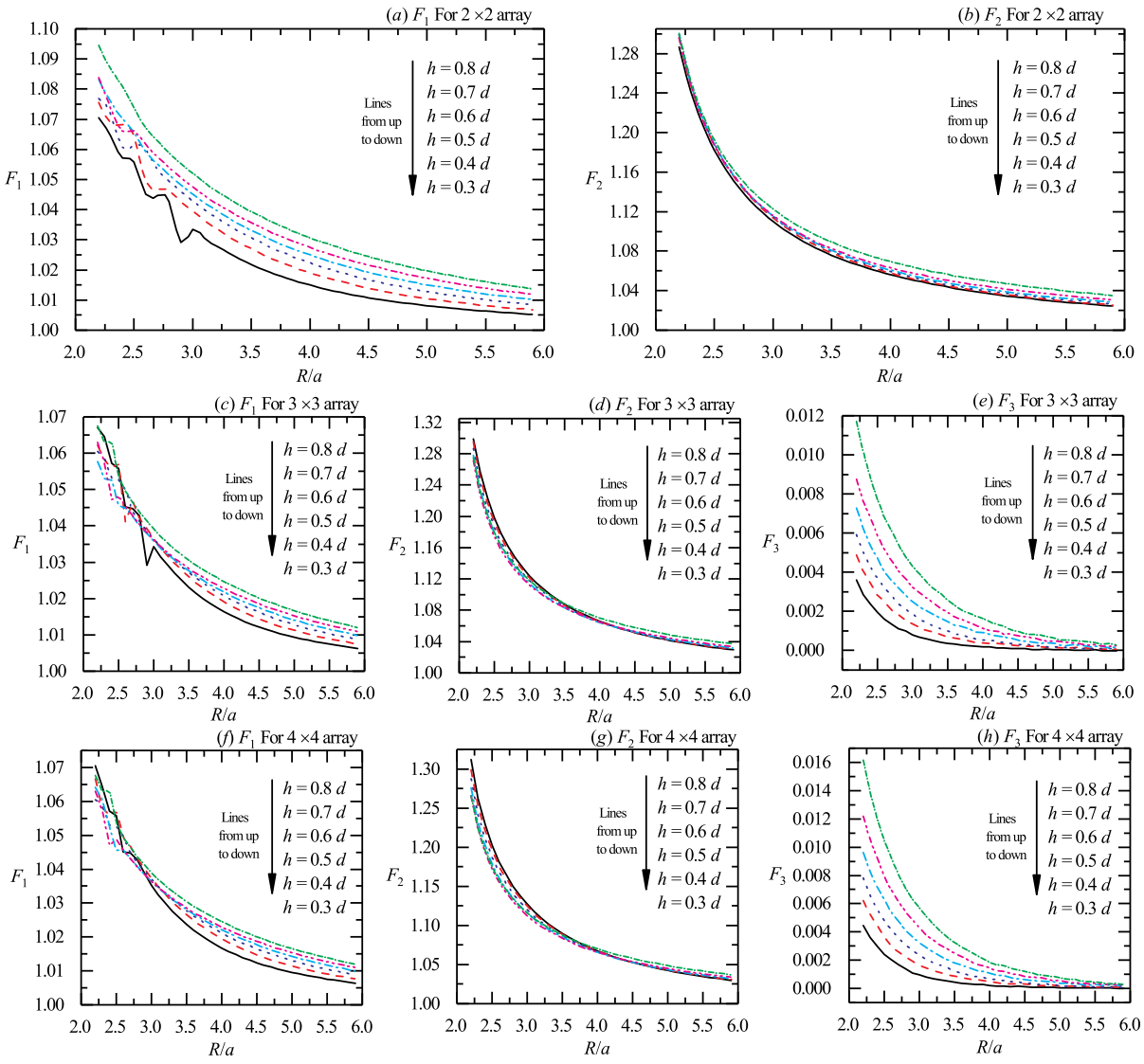

Fig. 14. Spectra of F_1, F_2 and F_3.

time. In order to overcome this obstacle, the following work has been done:

(*a*) Taking the simplest truncated two-cylinders model as an example, the influence of evanescent mode on hydrodynamic coefficient is studied, and the fast calculation formula of hydrodynamic coefficient of the truncated two-cylinders model is given.

(*b*) An array with a large number of truncated cylinders are divided into three types (case A, B, C). A fast formula for calculating the added mass of an oscillating cylinder in the three types array caused by the evanescent mode is given.

(*c*) The fast calculation method of an array with a large number of cylinders is summarized. The research provides guidance for the approximate evaluation of hydrodynamic characteristics of a large number of cylinders in engineering and also has guiding significance for the development of hydrodynamic calculation method of truncated cylindrical array with relative motion between cylinders in the presence of incident waves.

CRediT authorship contribution statement

Xiaohui Zeng: Conceptualization, Methodology, Supervision, Writing – original draft, Writing – review & editing. **Yuanshun Kang:** Conceptualization, Methodology, Software, Data curation, Writing – original draft, Writing – review & editing. **Guangyuan Wang:** Data curation, Validation, Writing – review & editing. **Zhen Xue:** Validation, Writing – review & editing. **FaJun Yu:** Validation, Writing – review & editing.

Declaration of competing interest

The authors declare that they have no known competing financial interests or personal relationships that could have appeared to influence the work reported in this paper.

Acknowledgments

This work was supported by the National Natural Science Foundation of China (grant no. 11672306), the National Natural Science Foundation of China Youth Fund (grant no. 51809055), the Young scientist foundation of Harbin Engineering University (grant no. 79000001), and the open fund of the State Key Laboratory of coastal and offshore engineering, Dalian University of Technology (grant no. LP21V1).

Table 1
Query table of function c.

d/a	$h/d=0.1$	$h/d=0.2$	$h/d=0.3$	$h/d=0.4$	$h/d=0.5$	$h/d=0.6$	$h/d=0.7$	$h/d=0.8$	$h/d=0.9$
6	1.26	2.33	3.99	5.61	6.97	8.06	8.57	7.78	5.57
8	1.78	3.50	6.24	9.14	11.83	14.21	15.63	14.43	9.98
10	2.39	4.89	9.01	13.51	17.81	21.85	24.73	23.48	16.08
12	3.13	6.62	12.41	18.67	24.54	30.22	34.81	34.05	23.51
14	4.04	8.77	16.51	24.49	31.59	38.49	44.67	44.93	31.68
16	5.17	11.44	21.35	30.82	38.57	46.02	53.36	54.98	39.94
18	6.55	14.72	26.97	37.53	45.20	52.43	60.34	63.44	47.76
20	8.24	18.71	33.40	44.50	51.30	57.61	65.50	70.04	54.82
22	10.31	23.54	40.66	51.66	56.84	61.63	69.04	74.87	61.09
24	12.81	29.30	48.79	58.98	61.88	64.72	71.32	78.29	66.72
26	15.78	36.07	57.80	66.46	66.50	67.13	72.77	80.79	71.99
28	19.25	43.91	67.66	74.05	70.80	69.08	73.75	82.81	77.29
32	27.44	62.34	89.27	89.29	78.66	72.40	75.51	87.21	89.73
36	35.90	81.94	110.69	103.10	85.35	75.44	78.12	93.98	107.97
40	41.46	96.01	125.31	111.75	89.29	77.76	81.82	104.66	136.87

Appendix

The elements of the isolated cylinder diffraction transfer matrix $\mathbf{B}_j^E$ can be expressed as follows:

$$B_j^E(m)=\begin{cases}-\dfrac{J'_m(k_0a)}{H'_m(k_0a)}+\dfrac{D_{m0s}\cdot\cosh(k_0H)}{N_0^{1/2}\cdot H_m'^{(1)}(k_0a)\cdot e^{im(\pi/2-\beta)}}, & q=0,n=0\\ \dfrac{D_{mqs}}{N_q^{1/2}\cdot K'_m(k_qa)\cdot e^{im\cdot(\pi/2-\beta)}}, & q\geqslant 1,n=0\\ \dfrac{D^e_{m0ns}\cdot\cosh(k_0H)}{H_m'^{(1)}(k_0a)\cdot N_0^{1/2}}, & q=0,n\geqslant 1\\ \dfrac{D^e_{mqns}}{N_q^{1/2}\cdot K'_m(k_qa)}, & q\geqslant 1,n\geqslant 1,q\neq n\\ -\dfrac{I'_m(k_na)}{K'_m(k_na)}+\dfrac{B^e_{mqp}}{N_q^{1/2}\cdot K'_m(k_qa)}, & q\geqslant 1,n\geqslant 1,\ q=n\end{cases} \tag{A.1}$$

and similarity, the elements of the diffraction transfer matrix $\mathbf{B}_j^C$ in the core region can be expressed as follows:

$$B_j^C(m)=\begin{cases}\dfrac{C_{m0s}}{2a^{|m|}\cdot e^{im\cdot(\pi/2-\beta)}}, & n=0,p=0\\ \dfrac{C_{mns}}{I_m\left(\frac{n\pi a}{H-h}\right)\cdot e^{im\cdot(\pi/2-\beta)}}\cdot\cos\dfrac{n\pi(z+H)}{H-h}, & n\geqslant 1,p=0\\ \dfrac{C^e_{m0ps}}{2a^{|m|}}, & n=0,p\geqslant 1\\ \dfrac{C^e_{mnps}}{I_m\left(\frac{n\pi a}{H-h}\right)}\cdot\cos\dfrac{n\pi(z+H)}{H-h}, & n\geqslant 1,p\geqslant 1\end{cases}. \tag{A.2}$$

where C_{mns} and D_{mqs} are unknown diffraction coefficients of truncated isolated cylinder in propagating mode, see Zeng and Tang (2013) and Zeng et al. (2016) for more details. C^e_{mnps} and D^e_{mqns} are unknown diffraction coefficients of truncated isolated cylinder in the evanescent mode, which can be found in Yilmaz et al. (2001).

The expression of the radiation velocity potential of cylinder j in the core region is

$$\varphi^j_{Rs-C}(r_j,\theta_j,z)=\sum_{m=-\infty}^{\infty}\left(\frac{1}{2}C_{m0s}\left(\frac{r_j}{a}\right)^{|m|}+\sum_{n=1}^{\infty}C_{mns}\cdot\frac{I_m\left(\frac{n\pi r_j}{H-h}\right)}{I_m\left(\frac{n\pi a}{H-h}\right)}\cdot\cos\frac{n\pi(z+H)}{H-h}+\Lambda_{ms}(r_j,z)\right)\cdot e^{im\theta}. \tag{A.3}$$

At last, the query table of function c is shown in Table 1.

References

Abramowitz, M., Stegun, I.A., 1964. Handbook of Mathematical Functions with Formulas, Graphs, and Mathematical Tables, vol. 55. US Government printing office.

Bennetts, L.G., Peter, M.A., Montiel, F., 2017. Localisation of Rayleigh–Bloch waves and damping of resonant loads on arrays of vertical cylinders. J. Fluid Mech. 813, 508–527.

Bhatta, D., Rahman, M., 2003. On scattering and radiation problem for a cylinder in water of finite depth. Internat. J. Engrg. Sci. 41, 931–967.

Chatjigeorgiou, I.K., 2018. Water wave trapping in a long array of bottomless circular cylinders. Wave Motion 83, 25–48.

Chatjigeorgiou, I.K., Chatziioannou, K., Mazarakos, T., 2019. Near trapped modes in long array of truncated circular cylinders. J. Waterw. Port Coast. Ocean Eng. 145, 04018035.

Child, B., Venugopal, V., 2010. Optimal configurations of wave energy device arrays. Ocean Eng. 37, 1402–1417.

Cong, P., Chen, L., Gou, Y., 2020. Hydrodynamic interaction among multiple columns in front of a vertical wall. Ocean Eng. 197, 106877.

Cong, P., Teng, B., Bai, W., Ning, D., Liu, Y., 2021. Wave power absorption by an oscillating water column (OWC) device of annular cross-section in a combined wind-wave energy system. Appl. Ocean Res. 107, 102499.

Garnaud, X., Mei, C.C., 2009. Wave-power extraction by a compact array of buoys. J. Fluid Mech. 635, 389.

Garrett, C., 1971. Wave forces on a circular dock. J. Fluid Mech. 46, 129–139.

Goteman, M., Engstrom, J., Eriksson, M., Isberg, J., 2015. Optimizing wave energy parks with over 1000 interacting point-absorbers using an approximate analytical method. Int. J. Marine Energy 10, 113–126.

Göteman, M., Giassi, M., Engström, J., Isberg, J., 2020. Advances and challenges in wave energy park optimization—A review. Front. Energy Res. 8, 26.

Grice, J.R., Taylor, P.H., Taylor, E.T., 2015a. Second-order statistics and'designer' waves for violent free-surface motion around multi-column structures. Philos. Trans. A Math. Phys. Eng. Sci. 373, 20140113.

Grice, J.R., Taylor, P.H., Taylor, E.T., Zang, J., Walker, D.A.G., 2015b. Extreme wave elevations beneath offshore platforms, second order trapping, and the near flat form of the quadratic transfer functions. Comput. & Fluids 119, 13–25.

Kagemoto, H., Yue, D.K., 1986. Interactions among multiple three-dimensional bodies in water waves: an exact algebraic method. J. Fluid Mech. 166, 189–209.

Kang, A., Zhu, B., Lin, P., Ju, J., Zhang, J., Zhang, D., 2020. Experimental and numerical study of wave-current interactions with a dumbbell-shaped bridge cofferdam. Ocean Eng. 201, 107433.

Kashiwagi, M., 2000. Hydrodynamic interactions among a great number of columns supporting a very large flexible structure. J. Fluids Struct. 14, 1013–1034.

Kashiwagi, M., 2017. Hydrodynamic interactions of multiple bodies with water waves. Int. J. Offshore Polar Eng. 27, 113–122.

Kim, M.-H., 1993. Interaction of waves with N vertical circular cylinders. J. Waterw. Port Coast. Ocean Eng. 119, 671–689.

Konispoliatis, D., Mavrakos, S., 2016. Hydrodynamic analysis of an array of interacting free-floating oscillating water column (OWC's) devices. Ocean Eng. 111, 179–197.

Konispoliatis, D., Mazarakos, T., Mavrakos, S., 2016. Hydrodynamic analysis of three–unit arrays of floating annular oscillating–water–column wave energy converters. Appl. Ocean Res. 61, 42–64.

Linton, C., Evans, D., 1990. The interaction of waves with arrays of vertical circular cylinders. J. Fluid Mech. 215, 549–569.

Lu, W., Zhao, W., Taylor, P.H., Yang, J., Xiao, L., Li, X., 2020. Linearity and nonlinearity in wave run-up and air-gap response for a semi-submersible platform under irregular wave excitation. Appl. Ocean Res. 104, 102218.

Maniar, H., Newman, J., 1997. Wave diffraction by a long array of cylinders. J. Fluid Mech. 339, 309–330.

Mavrakos, S., 1991. Hydrodynamic coefficients for groups of interacting vertical axisymmetric bodies. Ocean Eng. 18, 485–515.

McNatt, J.C., Venugopal, V., Forehand, D., 2015. A novel method for deriving the diffraction transfer matrix and its application to multi-body interactions in water waves. Ocean Eng. 94, 173–185.

Miles, J., Gilbert, F., 1968. Scattering of gravity waves by a circular dock. J. Fluid Mech. 34, 783–793.
Murai, M., Kagemoto, H., Fujino, M., 1999. On the hydroelastic responses of a very large floating structure in waves. J. Marine Sci. Technol. 4, 123–153.
Ohkusu, M., 1974. Hydrodynamic forces on multiple cylinders in waves. In: Proceedings of International Symposium on the Dynamics of Marine Vehicles and Structures in Waves, 1974. Institute of Mechanical Engineers.
Poter, R., Evans, D.V., 2005. Embedded Rayleigh–Bloch surface waves along periodic rectangular arrays. Wave Motion 43, 29–50.
Sabuncu, T., Calisal, S., 1981. Hydrodynamic coefficients for vertical circular cylinders at finite depth. Ocean Eng. 8, 25–63.
Siddorn, P., Taylor, R.E., 2008. Diffraction and independent radiation by an array of floating cylinders. Ocean Eng. 35, 1289–1303.
Simon, M., 1982. Multiple scattering in arrays of axisymmetric wave-energy devices. Part 1. A matrix method using a plane-wave approximation. J. Fluid Mech. 120, 1–25.
Singh, J., Babarit, A., 2014. A fast approach coupling Boundary Element Method and plane wave approximation for wave interaction analysis in sparse arrays of wave energy converters. Ocean Eng. 85, 12–20.
Sriram, V., Agarwal, S., Schlurmann, T., 2021. Laboratory study on steep wave interactions with fixed and moving cylinder. Int. J. Offshore Polar Eng. 1053, 5381.
Thompson, I., Linton, C.M., Poter, R., 2008. A new approximation method for scattering by long finite arrays. Quart. J. Mech. Appl. Math. 61, 333–352.
Tromans, P.S., Anaturk, A.R., Hagemeijer, P., 1991. A new model for the kinematics of large ocean waves - application as a design wave. Ocean Waves 1, 154.
Wang, G., Zhang, M., Zhang, H., Yu, F., 2022. Wave diffraction from an array of porous cylinders with porous plates fixed inside. Ocean Eng. 245, 110327.
Williams, A., Abul-Azm, A., 1989. Hydrodynamic interactions in floating cylinder arrays—II. Wave radiation. Ocean Eng. 16, 217–263.
Xie, Z., Lu, L., Stoesser, T., Lin, J., Pavlidis, D., Salinas, P., Pain, C.C., Matar, O.K., 2017. Numerical simulation of three-dimensional breaking waves and its interaction with a vertical circular cylinder. J. Hydrodyn. 29, 800–804.
Yeung, R.W., 1981. Added mass and damping of a vertical cylinder in finite-depth waters. Appl. Ocean Res. 3, 119–133.
Yılmaz, O., Incecik, A., 1998. Analytical solutions of the diffraction problem of a group of truncated vertical cylinders. Ocean Eng. 25, 385–394.
Yilmaz, O., Incecik, A., Barltrop, N., 2001. Wave enhancement due to blockage in semi-submersible and TLP structures. Ocean Eng. 28, 471–490.
Zeng, X., Shi, M., Huang, S., 2016. Hydrodynamic interactions of water waves with a group of independently oscillating truncated circular cylinders. Acta Mech. Sinica 32, 773–791.
Zeng, X., Tang, S.-y., 2013. The hydrodynamic interactions of an array of truncated circular cylinders as each cylinder oscillates independently with different prescribed modes. J. Hydrodyn. 25, 27–38.
Zeng, X., Yu, F., Shi, M., Wang, Q., 2019. Fluctuation of magnitude of wave loads for a long array of bottom-mounted cylinders. J. Fluid Mech. 868, 244–285.
Zhang, Y., Teng, B., Gou, Y., 2021a. Nonlinear modelling of a point-absorber wave energy converter based on the weak-scatterer approximation. Ocean Eng. 239, 109924.
Zhang, Z., Yuan, H., Sun, S., Ren, H., 2021b. Hydrodynamic characteristics of a fixed semi-submersible platform interacting with incident waves by fully nonlinear method. Int. J. Naval Architect. Ocean Eng. 13, 526–544.
Zheng, S., Zhang, Y., Liu, Y., Iglesias, G., 2019. Wave radiation from multiple cylinders of arbitrary cross sections. Ocean Eng. 184, 11–22.